Supporting Information for

# Reversible Symmetry-Breaking Charge Separation in a Series of Perylenediimide Cyclophanes

Adam F. Coleman, Michelle Chen, Jiawang Zhou, Jae Yoon Shin, Yilei Wu, Ryan M. Young,*

and Michael R. Wasielewski*

Department of Chemistry and Institute for Sustainability and Energy at Northwestern, Northwestern University, Evanston, IL 60208-3113, USA

*Correspondence to: ryan.young@northwestern.edu, m-wasielewski@northwestern.edu

## Contents

## 1. Materials and Methods

### *a. Synthesis Details*

***p*-PDI$_2$, *m*-PDI$_2$**, and [1,1'-biphenyl]-4,4'-diyldimethanamine (**1**) were synthesized according to the literature.[1-2]

*Synthesis of* ***biph-PDI$_2$***

1,6,7,12-tetra(4-phenoxy)perylene-3,4:9,10-tetracarboxylic acid dianhydride (100 mg, 0.1 mmol), [1,1'-biphenyl]-4,4'-diyldimethanamine (**1**) (22 mg, 0.1 mmol), imidazole (1 g, 15 mmol), pyridine (10 mL, 124mmol), and toluene (200 mL) were mixed. The mixture was heated to 115 °C for 18 hours. After cooling to room temperature, 250 mL of 2 M HCl was added. The organic layer was collected and washed with water. The remaining aqueous layer was extracted with $CH_2Cl_2$, and the organic layer was collected. The solvent was removed from the combined organic layers under reduced pressure. The crude product was purified via column chromatography ($CH_2Cl_2$, silica) and HPLC (10mg, 8%).

$^1$H-NMR (600 MHz, 353 K, $C_2D_2Cl_4$): $\delta$ = 8.16 (s, 8H), 7.46 (d, J = 8.46 Hz, 8H), 7.40 (d, J = 8.22 Hz, 8H), 7.24 (d, J = 8.64 Hz, 16H), 6.81 (bs, 16H), 5.34 (bs, 8H), 1.34 (s, 72H) ppm

HRMS (APPI, positive mode, DCM): *m*/*z*: calculated for $C_{156}H_{137}N_4O_{16}$: 2322.0024 $[M+H]^+$, found: 2322.0010.

### *b. Broadband fs Fluorescence Up-Conversion Spectroscopy*

Femtosecond broadband fluorescence up-conversion spectroscopy was used to investigate the early time dynamics of transient fluorescence spectra. A Yb:KGW regenerative amplifier (Spirit, Spectra Physics, 1040-4) pumped a $\beta$-barium borate (BBO) based two-stage noncollinear optical parametric amplifier (Spirit-NOPA, Light Conversion Inc.) with a 1040 nm fundamental pulse (400 fs duration and 26 $\mu$J) at a 100 kHz. A 300 mm f.l. lens focused the NOPA output pulse onto a 1 mm quartz cell for sample excitation after delay by a computer-controlled delay stage. A reflective microscope objective (15x, 160 mm back focal length, Newport 50105-01) collected the fluorescence from the samples. The collected fluorescence image was collimated by a 90° off-axis parabolic mirror (2 inch diameter, 4 inch reflected f.l.)

and refocused onto a BBO crystal (type I, θ 23°, φ 90°, 1 mm thick) by an additional 90° off-axis parabolic mirror (2 inch diameter, 2 inch reflected f.l.). A different portion of the1040 nm fundamental pulse (9 $\mu$J) was used as a gate pulse and focused with a 100 mm f.l. lens onto the BBO crystal, crossing the fluorescence at an angle of 26°. Sum frequency generation of the fluorescence and the gate pulse emitting along the phase matching direction was dispersed on a NMOS linear image sensor (Hamamatsu, S3901-512Q) by a grating (600 groves/mm blazed at 300 nm). To remove the signal from polarization-dependent dynamics, the polarization of excitation pulse was set to a magic angle (54.7°) to the horizontally polarized gate pulse using a λ/2 waveplate. A mechanical chopper modulated the excitation pulse at 45 Hz, which enabled background noise subtraction in the NMOS sensor and unwanted signal from the gate pulse only. A motorized stage moved the sample to refresh the excitation volume in the sample during runtime. The time resolution is approximately 300 fs.

The excitation wavelength was tuned to 580 nm (~30 fs duration and ~300 nJ/pulse) samples, respectively. Optical densities of the samples were 0.9 at the absorption maxima. Data acquisition time was 30 second integration for one spectrum with averaging 6 spectra for each time delay. Comparing the transient fluorescence spectra to the steady-state fluorescence spectra confirmed that there was no re-absorption of fluorescence and no need for spectral corrections.

*c. Fitting Methodology*

Prior to kinetic analysis, the fs/nsTA and data were background/scatter-subtracted and chirp-corrected, and the similar data sets were spectrally merged (Surface Xplorer 4, Ultrafast Systems, LLC). Nanosecond infrared spectra were processed by Singular Value Decomposition (SVD). The thermal artifact contribution was isolated and the dataset reconstituted prior to the global analysis described below.

The kinetic analysis was performed using home written programs in MATLAB and was based on a global fit to selected wavelength/frequency kinetics. The time-resolution is given as $w$ = 300 fs (full width at half maximum, FWHM); the assumption of a uniform instrument response across the frequency domain and a fixed time-zero ($t_0$) are implicit in global analysis. Kinetic data from multiple different

wavelengths/frequencies were fit using the global analysis described below. Each wavelength/frequency was given an initial amplitude that is representative of the spectral intensity at time $t_0$ and varied independently to fit the data. The time/rate constants and $t_0$ are shared between the various kinetic data and are varied globally across the kinetic data in order to fit the models described in the text. We globally fit the dataset to a specified kinetic model and use the resultant populations to deconvolute the dataset and reconstruct species-associated spectra. The MATLAB program numerically the solves the differential equations through matrix methods, then convolutes the solutions with a Gaussian instrument response function with width *w* before employing a least-squares fitting using a Levenberg-Marquardt or Simplex method to find the parameters which result in matches to the kinetic data. Once the fit parameters are established, they are fed directly into the differential equations, which were solved for the populations of the states in model—i.e., *A(t)*, *B(t)*, and *C(t)*, etc. Finally, the raw data matrix (with all the raw data) is deconvoluted with the populations as functions of time to produce the spectra associated with each species.

Single-wavelength kinetic analysis is performed in Origin 2019 by fitting the time-dependent signals $S(t)$ to the convolution of Gaussian instrument response with temporal width *w* and (i) a multi-exponential decay with amplitudes $a_i$ and time constants $\tau_i$, (ii) a delta function with amplitude $a_0$, centered at the zero of pump-probe delay ($t_0$) to account for instrument-limited coherence artifacts, and (iii) offsets for before ($S_0$) and after ($S_0'$) $t_0$ to account for any signals present beyond the experimental window:

$$S(t) = e^{-t^2/w^2} * \begin{cases} S_0 & t < t_0 \\ S_0' + a_0\delta(t - t_0) + \sum_{i=1}^{N} a_i \exp[-(t - t_0)]/\tau_i & t \geq t_0 \end{cases} \quad \text{(S1)}$$

The time-resolution is given as $2w\sqrt{\ln 2}$ ~300 fs, FWHM for fsTA and fs up-conversion spectroscopies, ~500 fs for fsIR, ~10 ns for nsIR, and ~0.6 ns for nsTA experiments, respectively, while for psTRF is ~2% of the experimental time window.

## 2. Additional Steady-State Spectroscopy Data

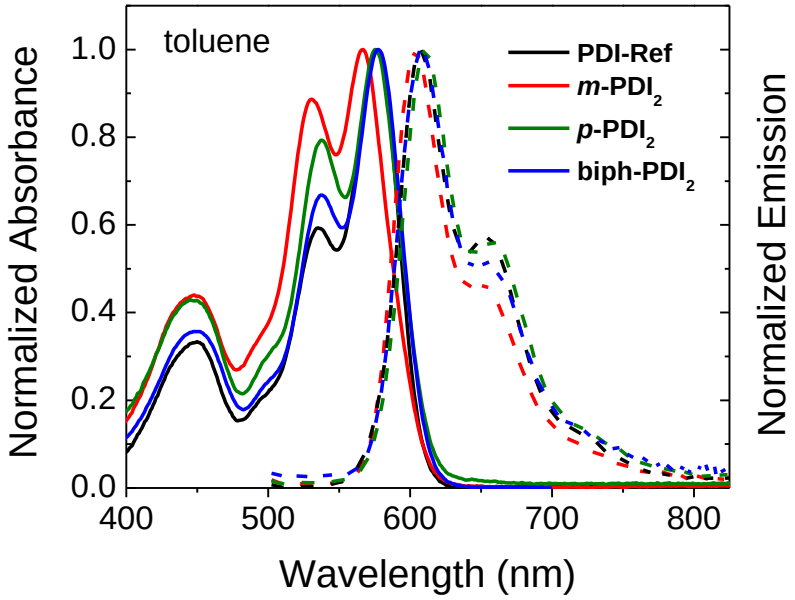


**Figure S1.** Absorption and emission spectra for **PDI-Ref, *m*-PDI$_2$**, ***p*-PDI$_2$**, and **biph-PDI$_2$** in toluene.

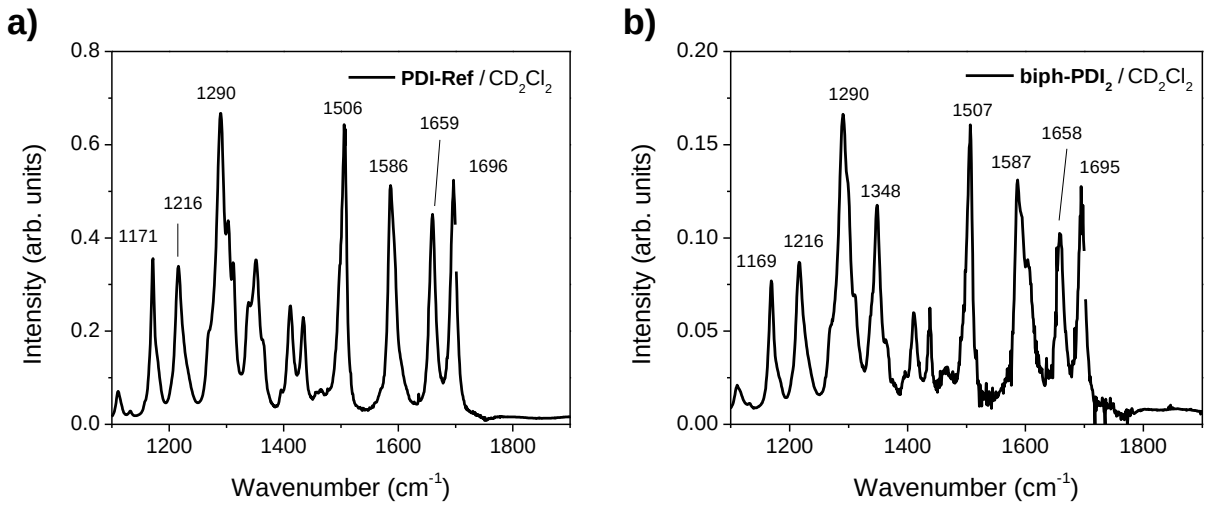


**Figure S2.** FTIR spectra of a) **PDI-Ref** and b) **biph-PDI$_2$** in $CD_2Cl_2$.

## 3. Electrochemistry

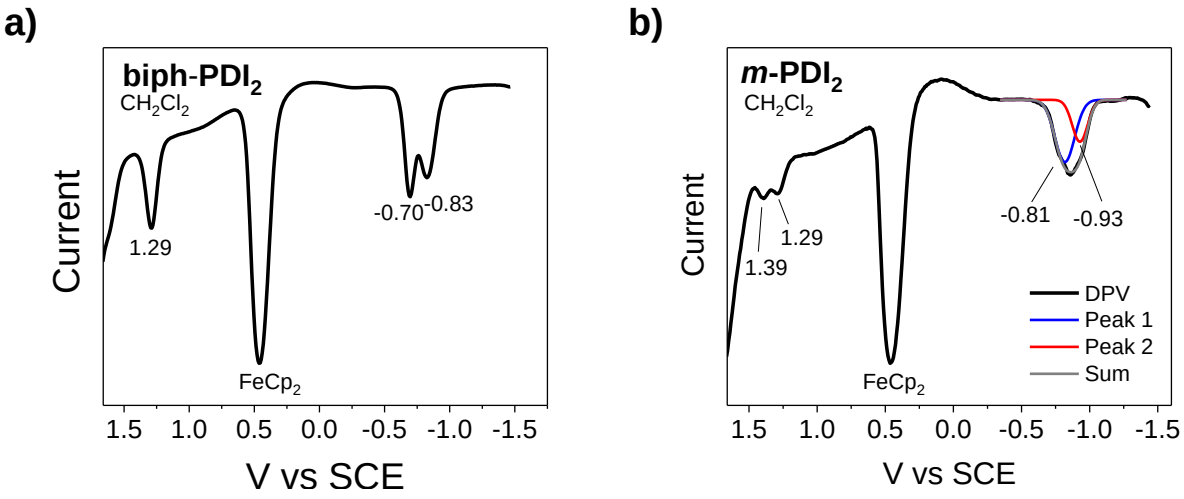


**Figure S3.** Differential Pulse Voltammograms of a) **biph-PDI$_2$** and b) ***m*-PDI$_2$** in $CH_2Cl_2$. Redox potentials for ***p*-PDI$_2$** and **PDI-Ref** have been reported previously.[3]

## 4. Additional Time-Resolved Spectroscopy Data.

### *a. fsTA Spectroscopy*

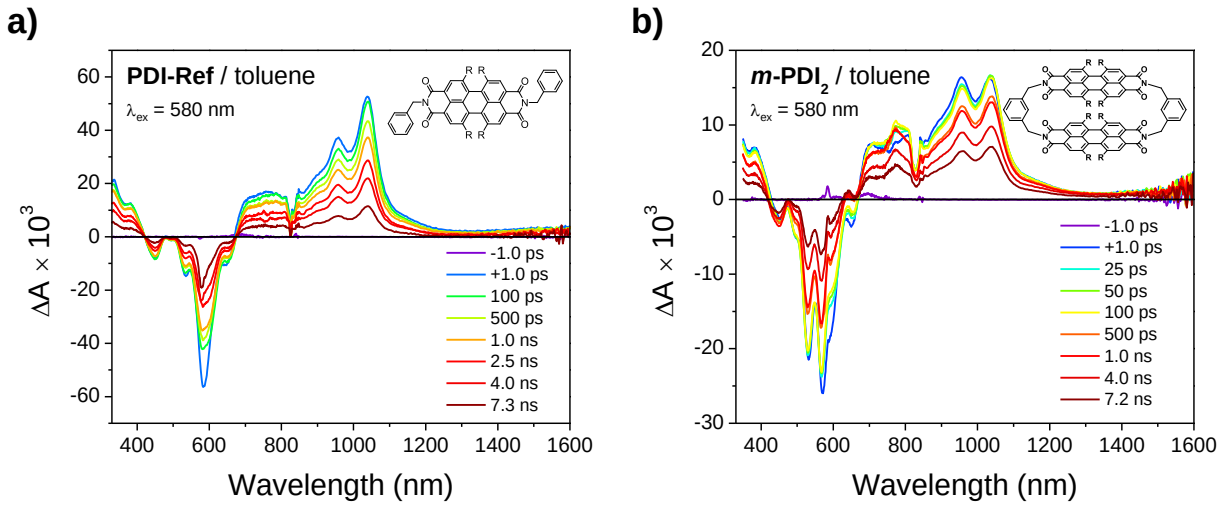


**Figure S4.** fsTA spectra of a) **PDI-Ref**, and ***m*-PDI$_2$** in toluene following $\lambda_{ex}$ = 580 nm excitation (1.0 μJ/pulse, ~120 fs) at 298 K. The depression near 830 nm is from scatter of the fundamental.

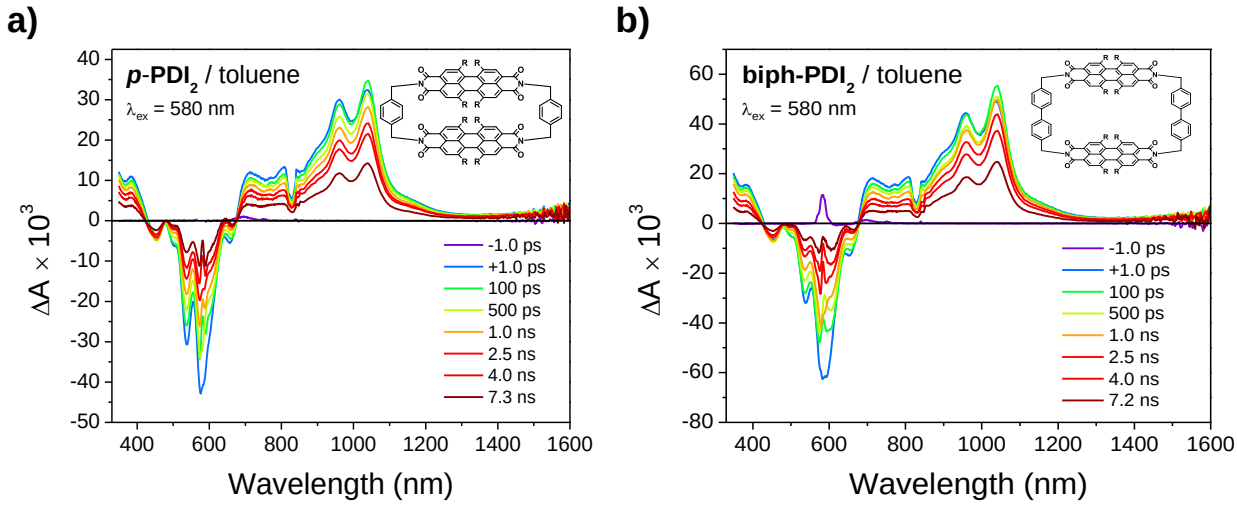


**Figure S5.** fsTA spectra of a) ***p*-PDI$_2$**, and **biph-PDI$_2$** in toluene following $\lambda_{ex}$ = 580 nm excitation (1.0 μJ/pulse, ~120 fs) at 298 K. The depression near 830 nm is from scatter of the fundamental.

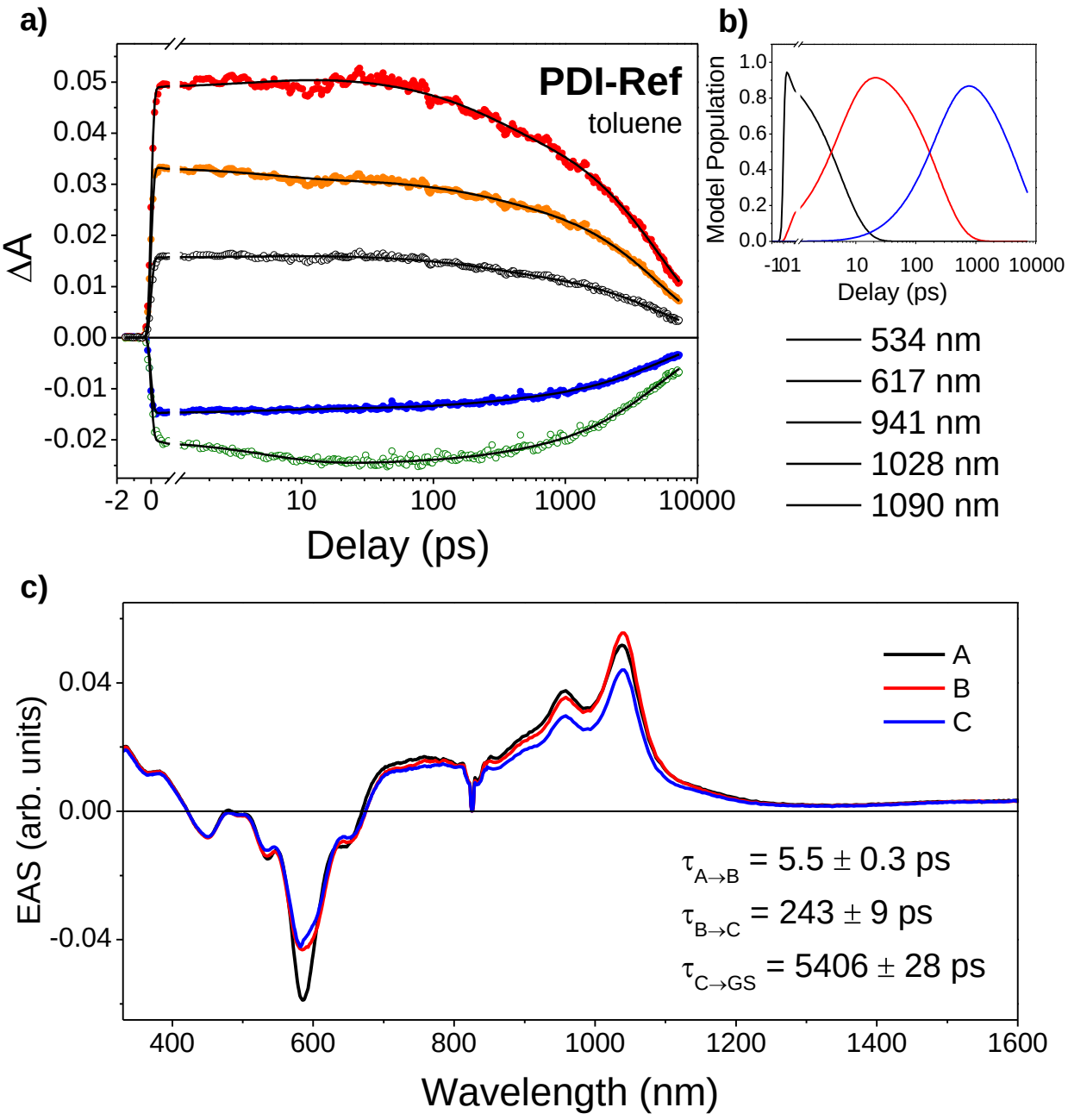


**Figure S6.** a) Global fits to selected fsTA wavelengths in **PDI-Ref** ($\lambda_{ex}$ = 580 nm) in toluene to a sequential A → B → ground state kinetic model. Fits are shown as solid lines. b) Solution to the kinetic model using the fit parameters. C) Evolution-associated spectra obtained from deconvolution of the data set with the kinetic fit solution. State A represents the unrelaxed *$S_1$ state, and state B is the relaxed $S_1$ state. The depression near 830 nm is from scatter of the fundamental.

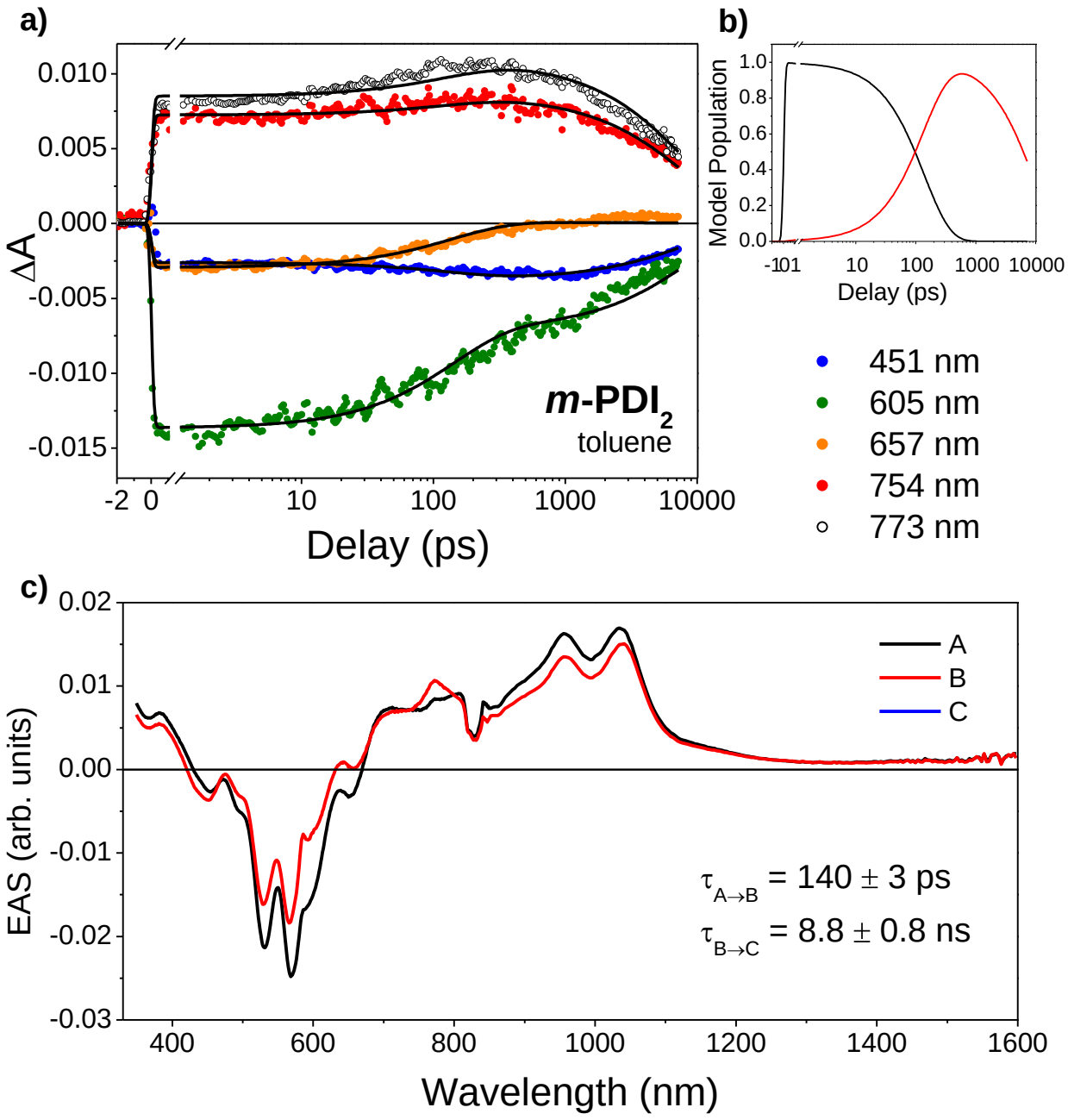


**Figure S7.** a) Global fits to selected fsTA wavelengths in ***m*-PDI₂** ($\lambda_{ex}$ = 580 nm) in toluene to a sequential A → B → ground state kinetic model. Fits are shown as solid lines. b) Solution to the kinetic model using the fit parameters. C) Evolution-associated spectra obtained from deconvolution of the data set with the kinetic fit solution. State A represents the vertical $S_1$ state, and state B shows co-existence of the $S_1$ and $tpPDI^{-\bullet}$ states as indicated by the characteristic anion feature at 790 nm and reduced stimulated emission. Triplet formation is neglected because the yield is very low. The data are analyzed using a full kinetic model in Section 5. The depression near 830 nm is from scatter of the fundamental.

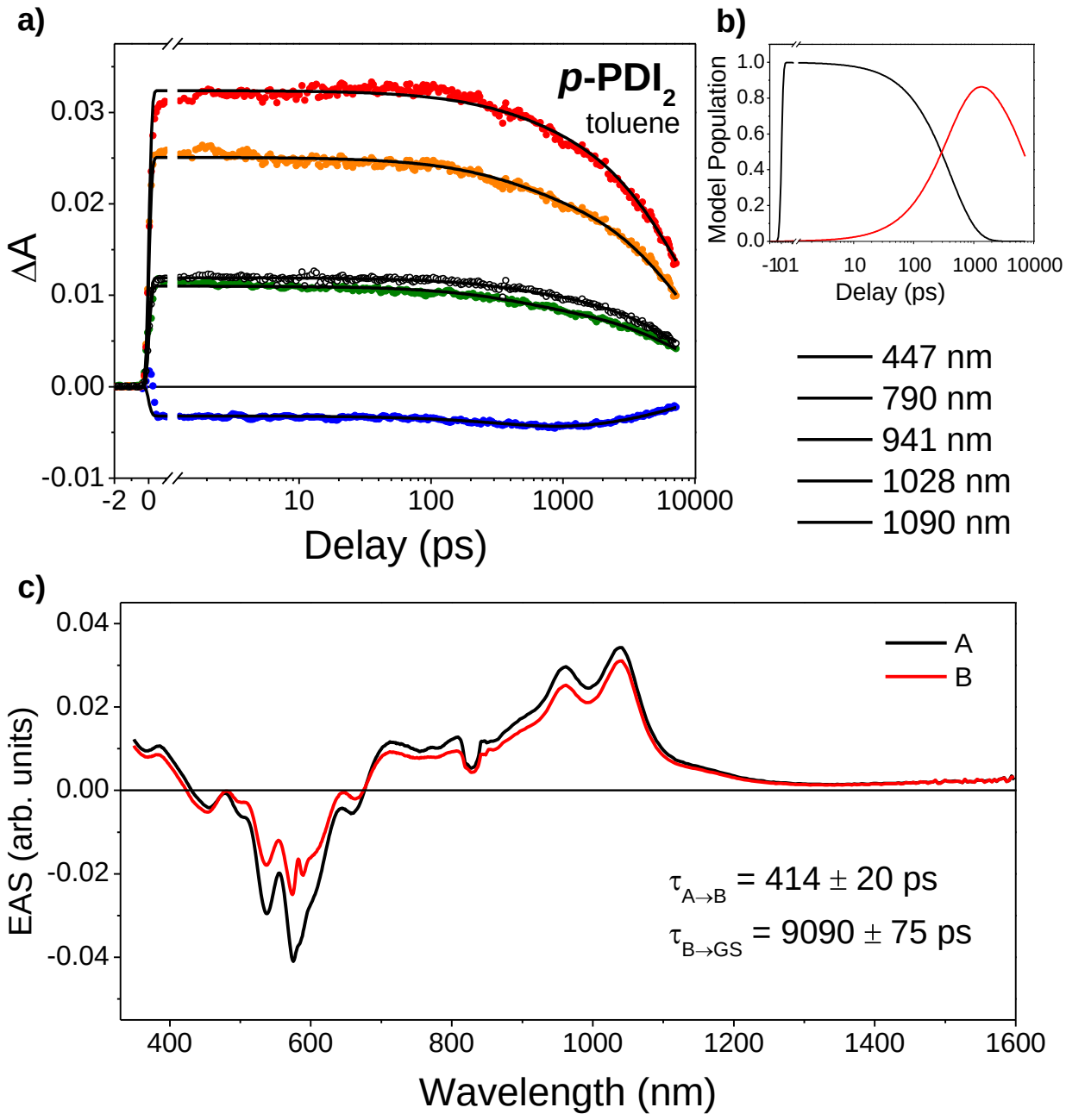


**Figure S8.** a) Global fits to selected fsTA wavelengths in ***p*-PDI$_2$** ($\lambda_{ex}$ = 580 nm) in toluene to a sequential A → B → ground state kinetic model. Fits are shown as solid lines. b) Solution to the kinetic model using the fit parameters. C) Evolution-associated spectra obtained from deconvolution of the data set with the kinetic fit solution. The various states represent the $S_1$ electronic state during state during multiple stages of structural relaxation/fluctuation with no indication of strong SB-CS. The depression near 830 nm is from scatter of the fundamental.

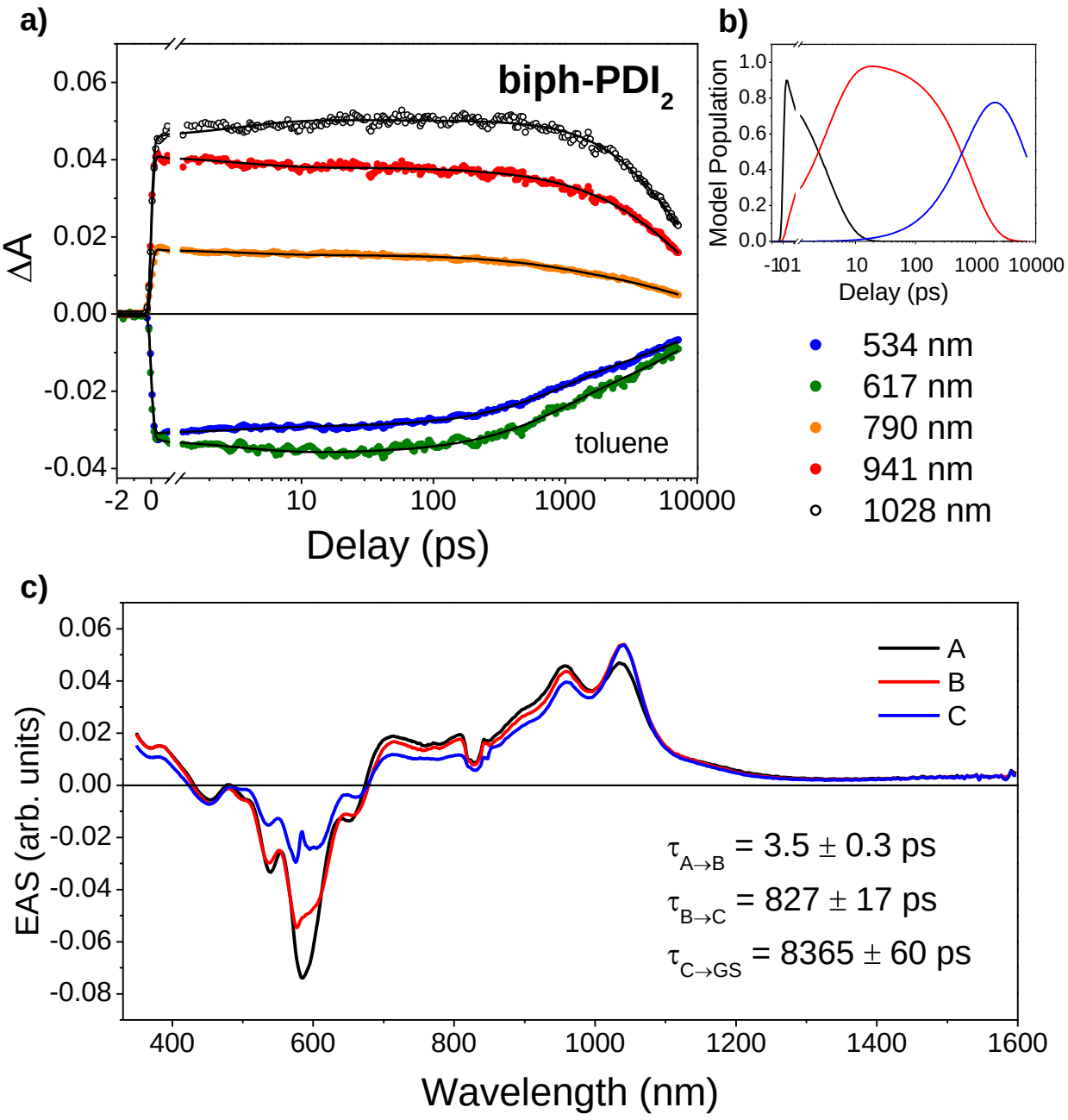


**Figure S9.** a) Global fits to selected fsTA wavelengths in **biph-PDI$_2$** ($\lambda_{ex}$ = 580 nm) in toluene to a sequential A → B → C → ground state kinetic model. Fits are shown as solid lines. b) Solution to the kinetic model using the fit parameters. C) Evolution-associated spectra obtained from deconvolution of the data set with the kinetic fit solution. The various states represent the $S_1$ electronic state during state during multiple stages of structural relaxation/fluctuation with no indication of strong SB-CS. The depression near 830 nm is from scatter of the fundamental.

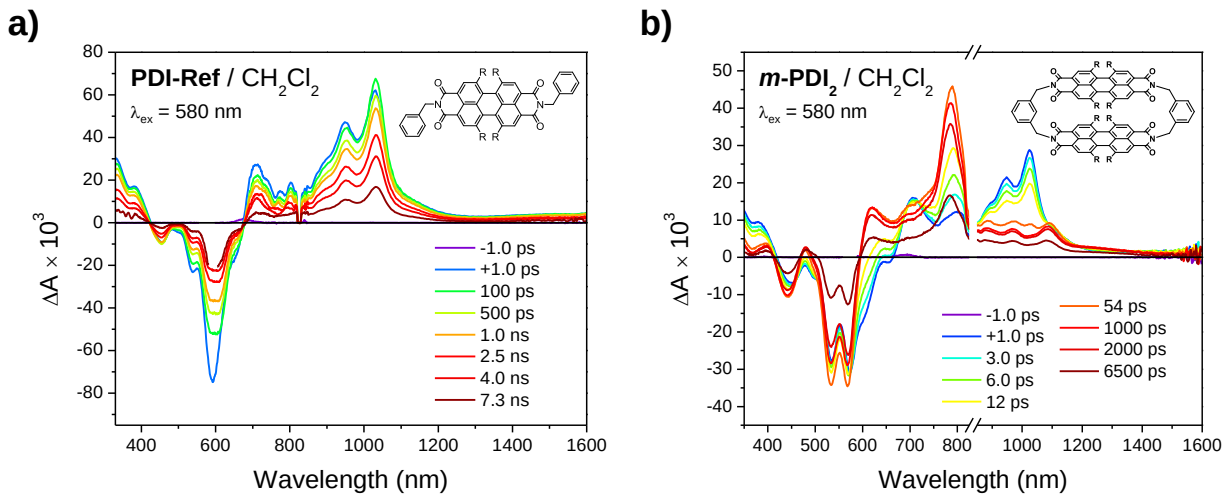


**Figure S10.** fsTA spectra of a) **PDI-Ref**, and ***m*-PDI$_2$** in $CH_2Cl_2$ following $\lambda_{ex}$ = 580 nm excitation (1.0 μJ/pulse, ~120 fs) at 298 K. The depression near 830 nm is from scatter of the fundamental. Pump scatter is masked for clarity.

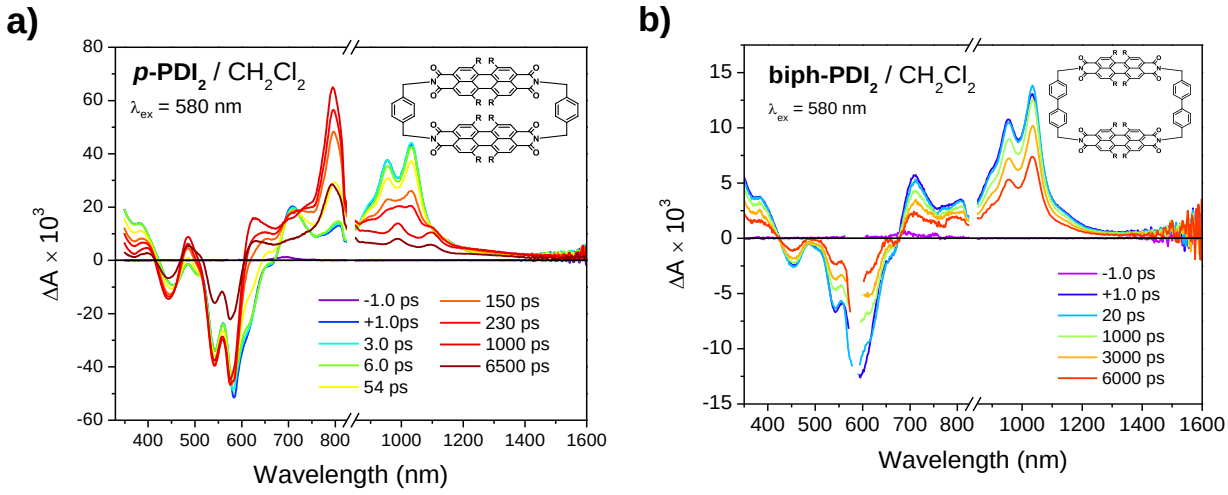


**Figure S11.** fsTA spectra of a) ***p*-PDI$_2$**, and **biph-PDI$_2$** in $CH_2Cl_2$ following $\lambda_{ex}$ = 580 nm excitation (1.0 μJ/pulse, ~120 fs) at 298 K. The depression near 830 nm is from scatter of the fundamental. Pump scatter is masked for clarity.

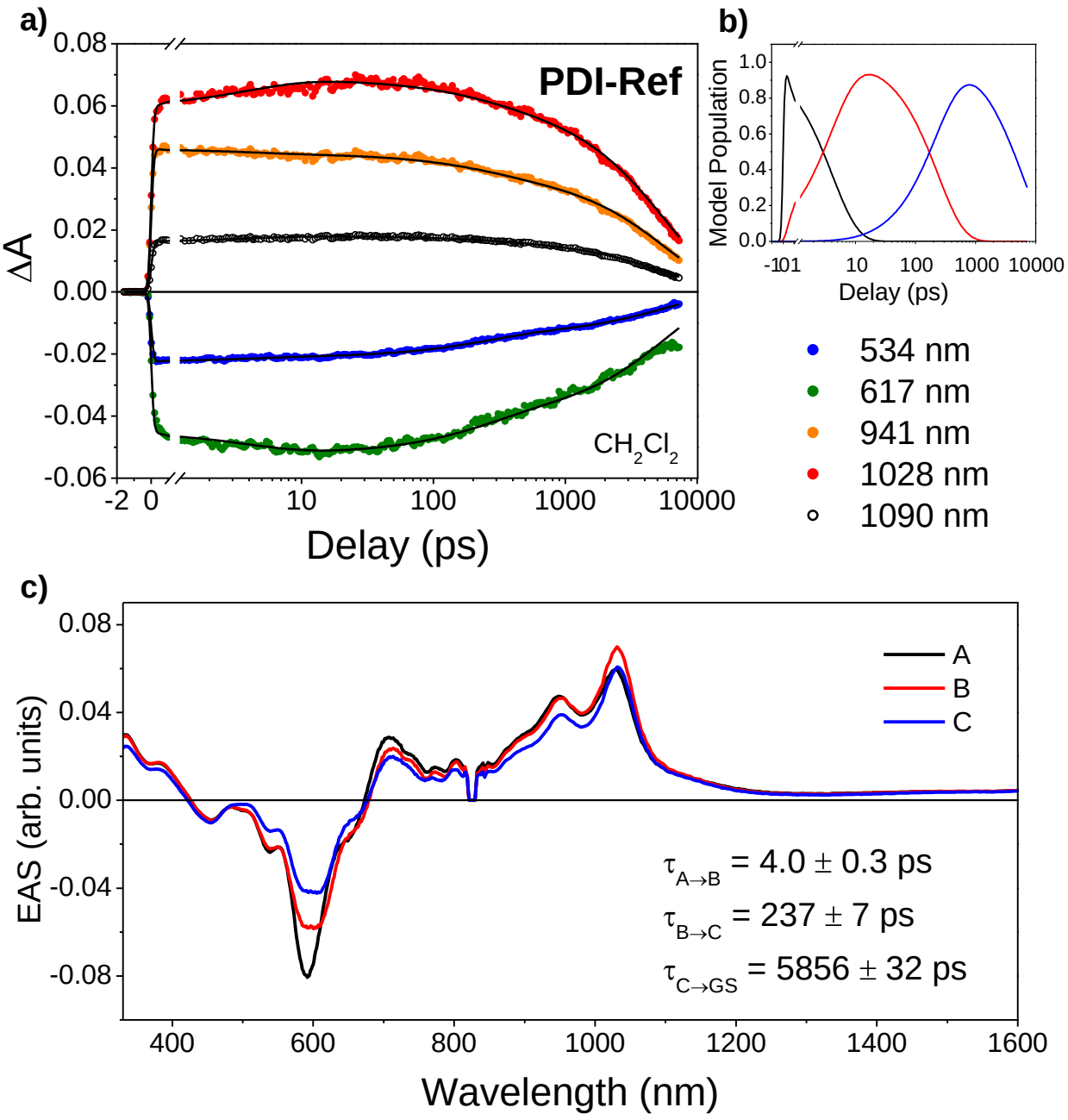


**Figure S12.** a) Global fits to selected fsTA wavelengths in **PDI-Ref** ($\lambda_{ex}$ = 580 nm) in $CH_2Cl_2$ to a sequential A → B → C → ground state kinetic model. Fits are shown as solid lines. b) Solution to the kinetic model using the fit parameters. C) Evolution-associated spectra obtained from deconvolution of the data set with the kinetic fit solution. State A represents the unrelaxed $^*S_1$ state, and state B is the relaxed $S_1$ state. The depression near 830 nm is from scatter of the fundamental.

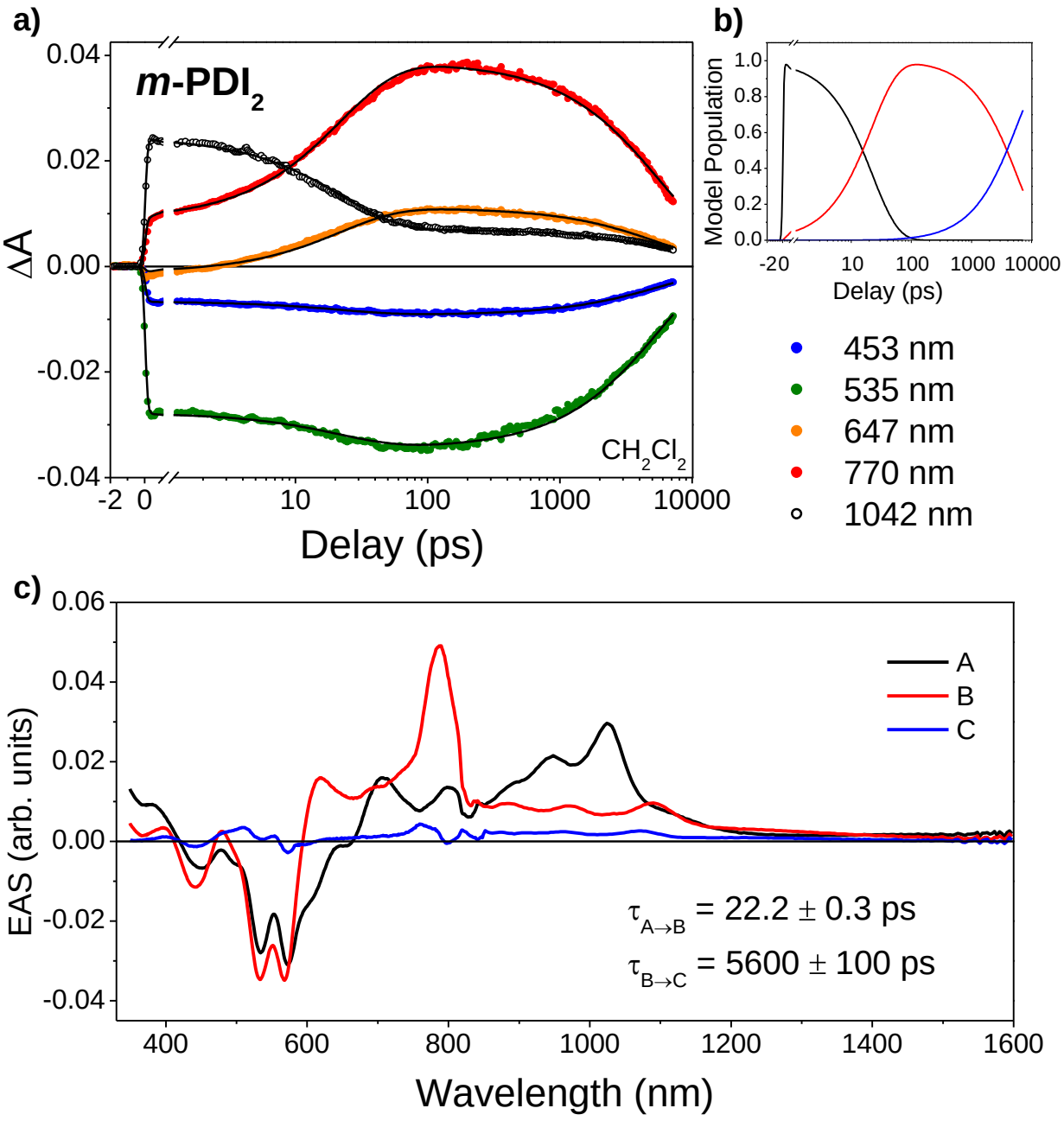


**Figure S13.** a) Global fits to selected fsTA wavelengths in ***m*-PDI$_2$** ($\lambda_{ex}$ = 580 nm) in $CH_2Cl_2$ to a sequential A → B → C kinetic model. Fits are shown as solid lines. b) Solution to the kinetic model using the fit parameters. C) Evolution-associated spectra obtained from deconvolution of the data set with the kinetic fit solution. State A represents the $S_1$ state, state B is the SB-CS state, and state C represents the $T_1$ state. The depression near 830 nm is from scatter of the fundamental.

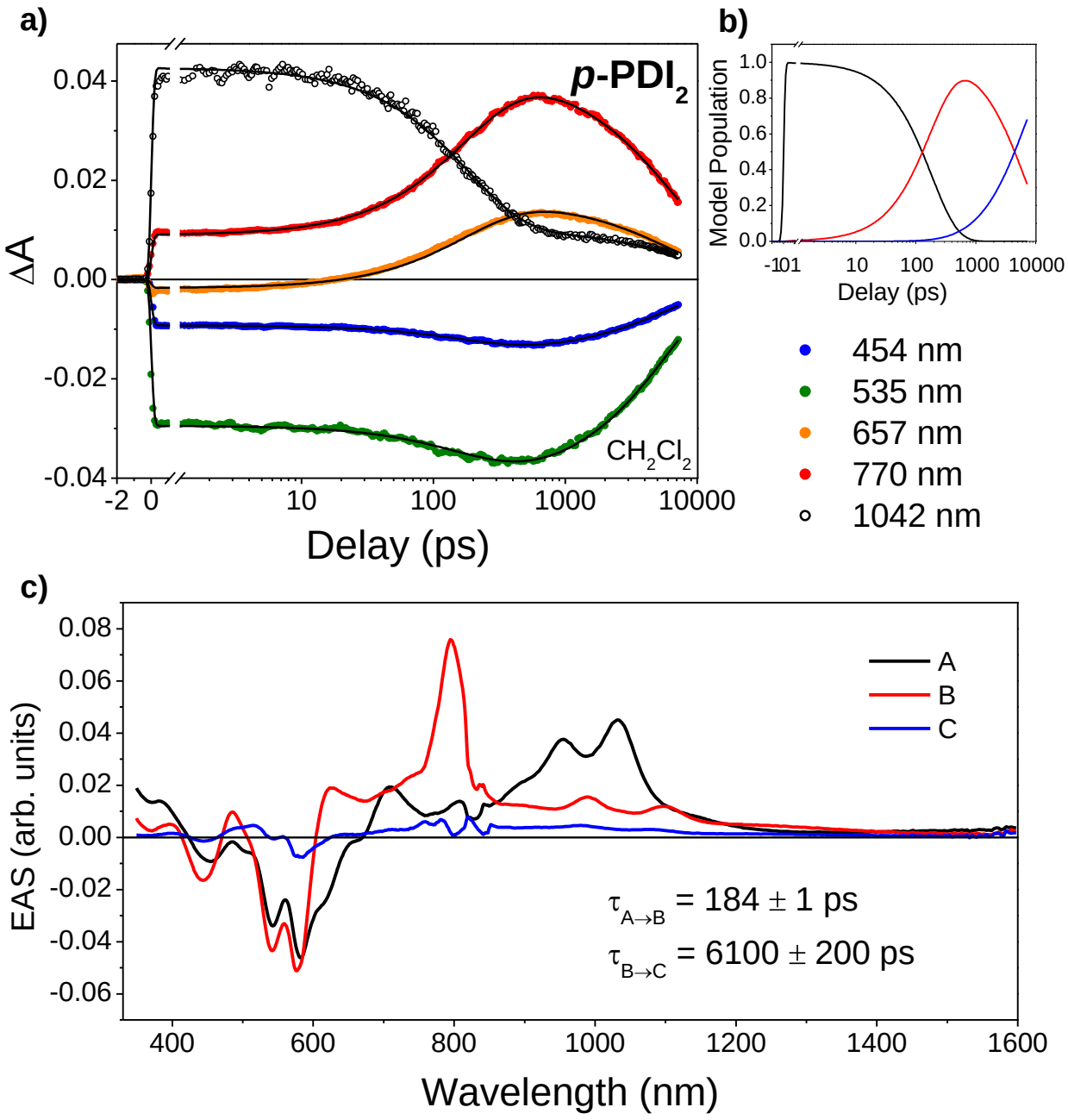


**Figure S14.** a) Global fits to selected fsTA wavelengths in ***p*-PDI$_2$** ($\lambda_{ex}$ = 580 nm) in $CH_2Cl_2$ to a sequential A → B → C kinetic model. Fits are shown as solid lines. b) Solution to the kinetic model using the fit parameters. C) Evolution-associated spectra obtained from deconvolution of the data set with the kinetic fit solution. State A represents the $S_1$ state, state B is the SB-CS state, and state C represents the $T_1$ state. The depression near 830 nm is from scatter of the fundamental.

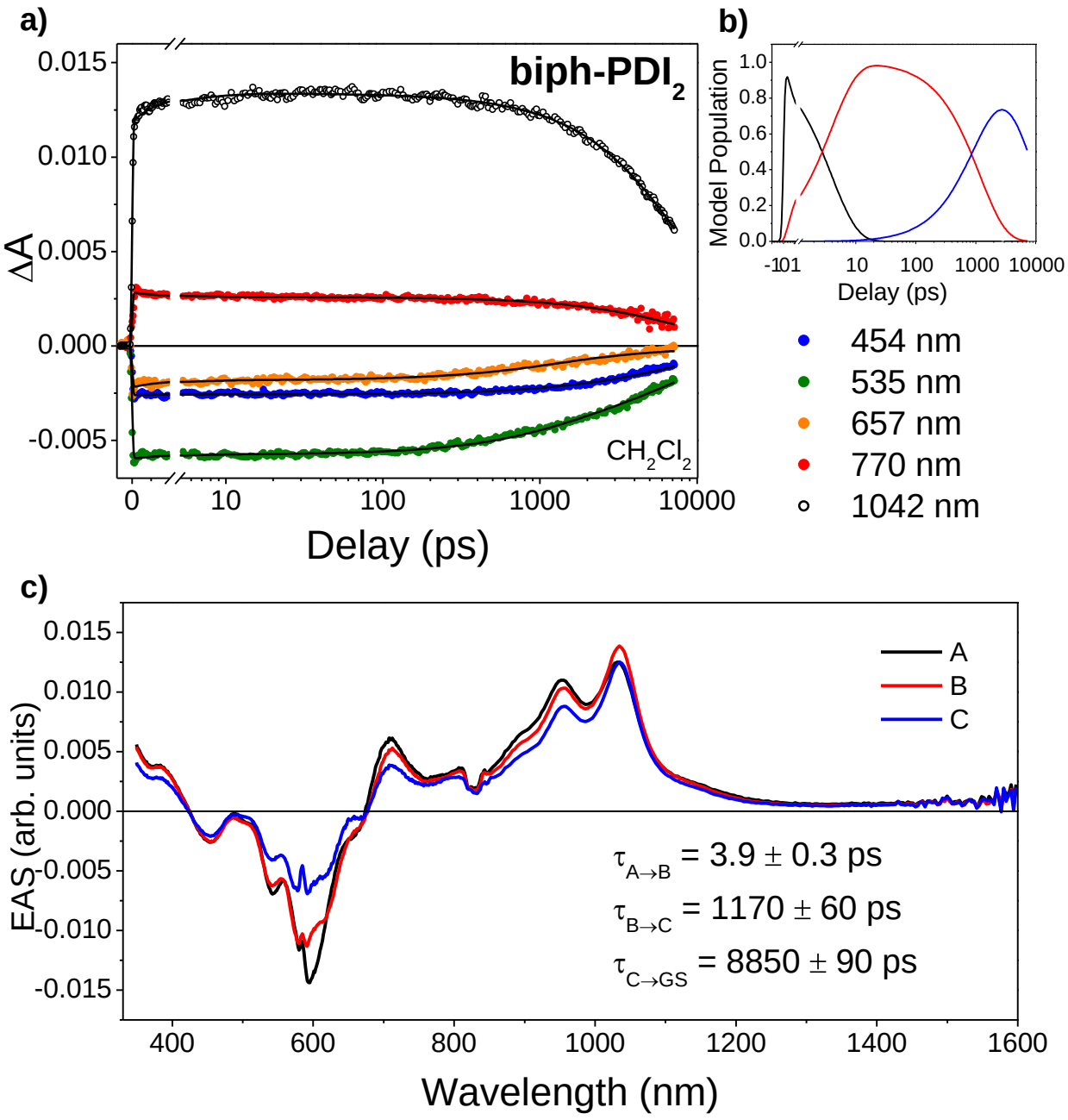


**Figure S15.** a) Global fits to selected fsTA wavelengths in **biph-PDI$_2$** ($\lambda_{ex}$ = 580 nm) in $CH_2Cl_2$ to a sequential A → B → C → ground state kinetic model. Fits are shown as solid lines. b) Solution to the kinetic model using the fit parameters. C) Evolution-associated spectra obtained from deconvolution of the data set with the kinetic fit solution. The various states represent the $S_1$ electronic state during state during multiple stages of structural relaxation/fluctuation with no indication of strong SB-CS; this process is much slower and is only visible in the nsTA data. The depression near 830 nm is from scatter of the fundamental.

*Variable Temperature fsTA (VT-fsTA)*

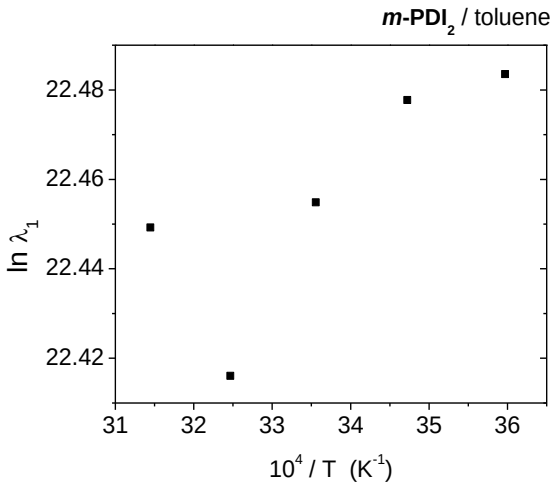


**Figure S16.** Arrhenius plot for the rate constant ($\lambda_1$) obtained from fitting the fsTA data for ***m*-PDI$_2$** in toluene at 657 nm to a single exponential decay as a function of temperature from 278 K to 318 K. No apparent trend is observed. Sample degradation occurred at higher temperatures. The slower process ($k_2$) observed in $CH_2Cl_2$ below is not observed in toluene as it is much slower.

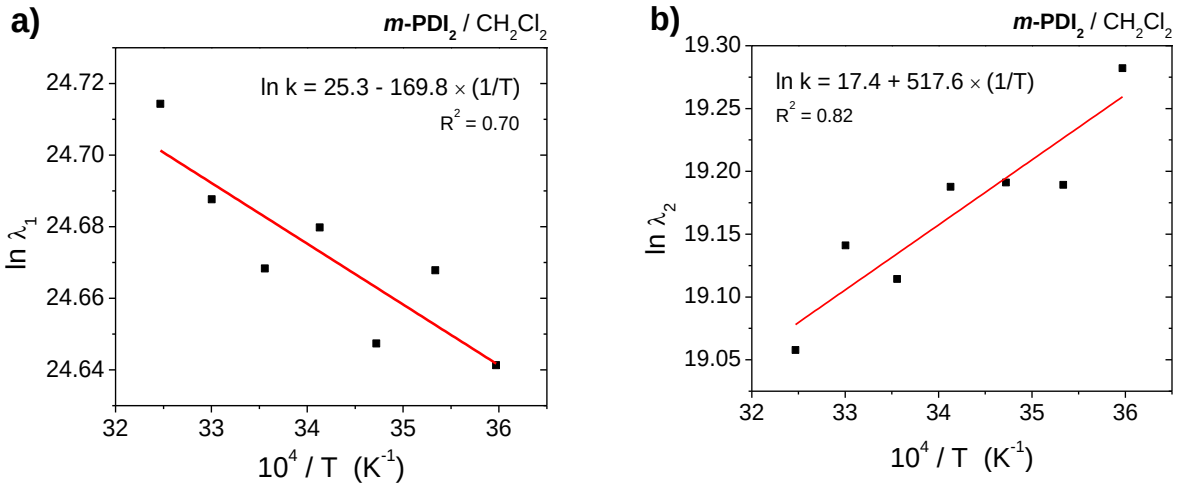


**Figure S17.** Arrhenius plots for a) the first ($\lambda_1$) and b) second ($\lambda_2$) rate constants obtained from fitting the fsTA data for ***m*-PDI$_2$** in $CH_2Cl_2$ at 657 nm to a sequential A → B → C model as a function of temperature from 278 K to 308 K. The positive slope in b) suggests a negative activation energy and strongly implies the presence of an excited-state equilibrium.

*b. nsTA Spectroscopy*

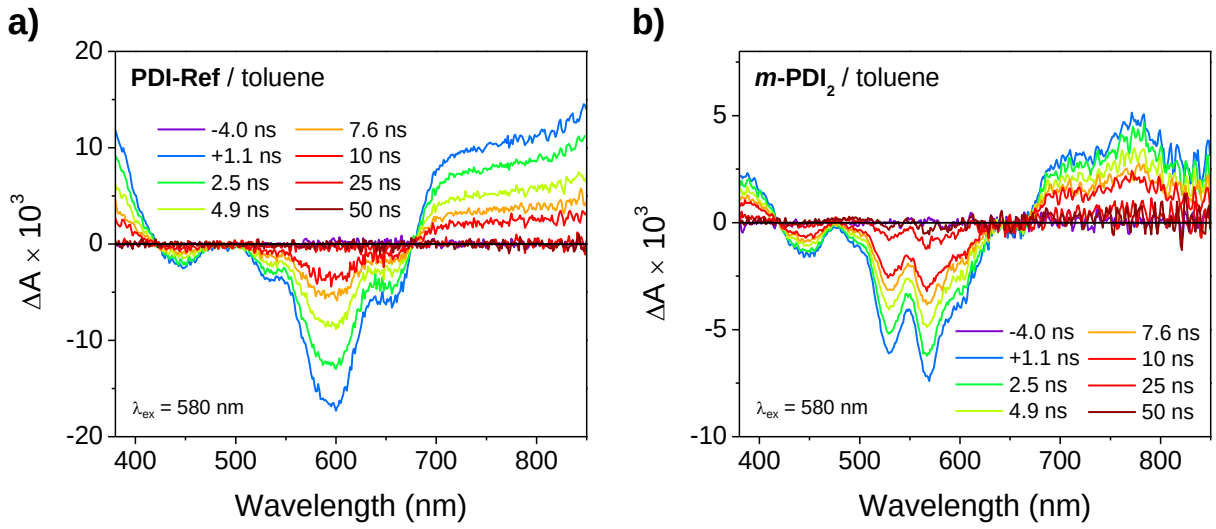


**Figure S18.** nsTA spectra of a) **PDI-Ref**, and ***m*-PDI$_2$** in toluene following $\lambda_{ex}$ = 580 nm excitation (1.0 μJ/pulse, ~120 fs) at 298 K.

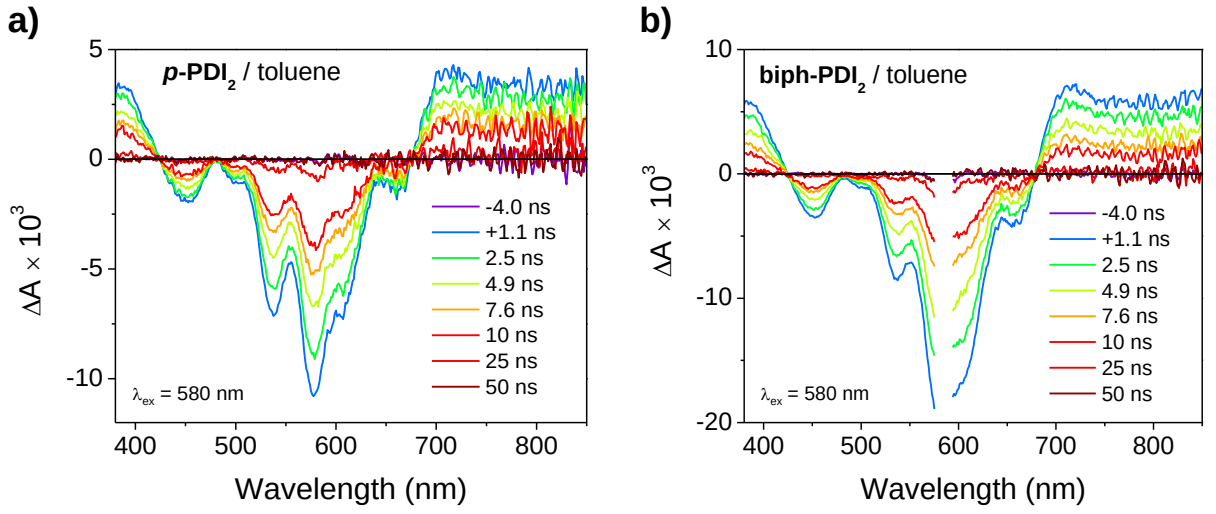


**Figure S19.** nsTA spectra of a) ***p*-PDI$_2$**, and **biph-PDI$_2$** in toluene following $\lambda_{ex}$ = 580 nm excitation (1.0 μJ/pulse, ~120 fs) at 298 K.

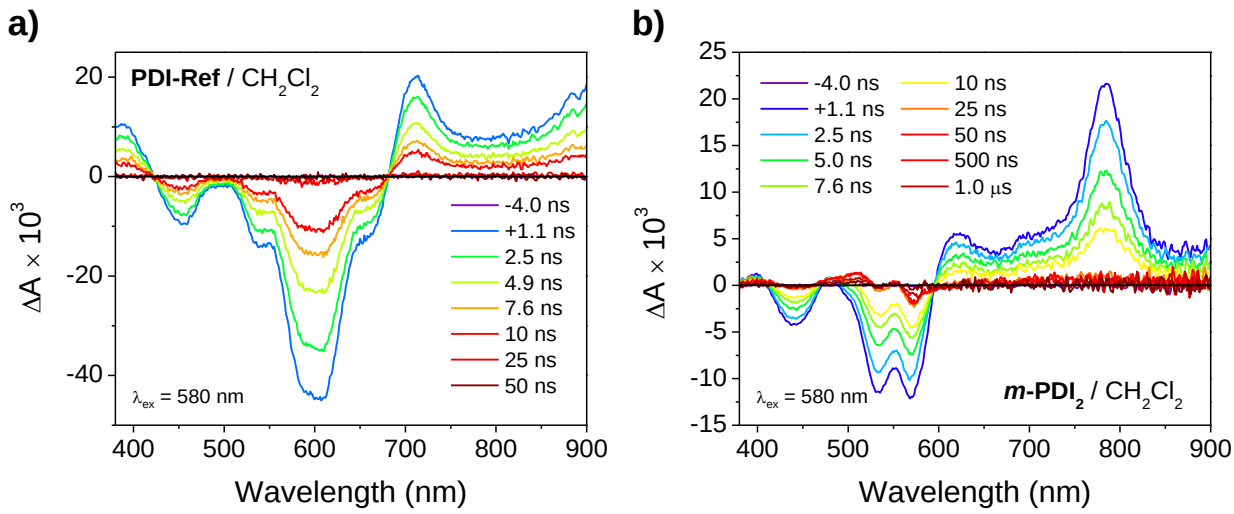


**Figure S20.** nsTA spectra of a) **PDI-Ref**, and ***m*-PDI$_2$** in $CH_2Cl_2$ following $\lambda_{ex}$ = 580 nm excitation (1.0 μJ/pulse, ~120 fs) at 298 K.

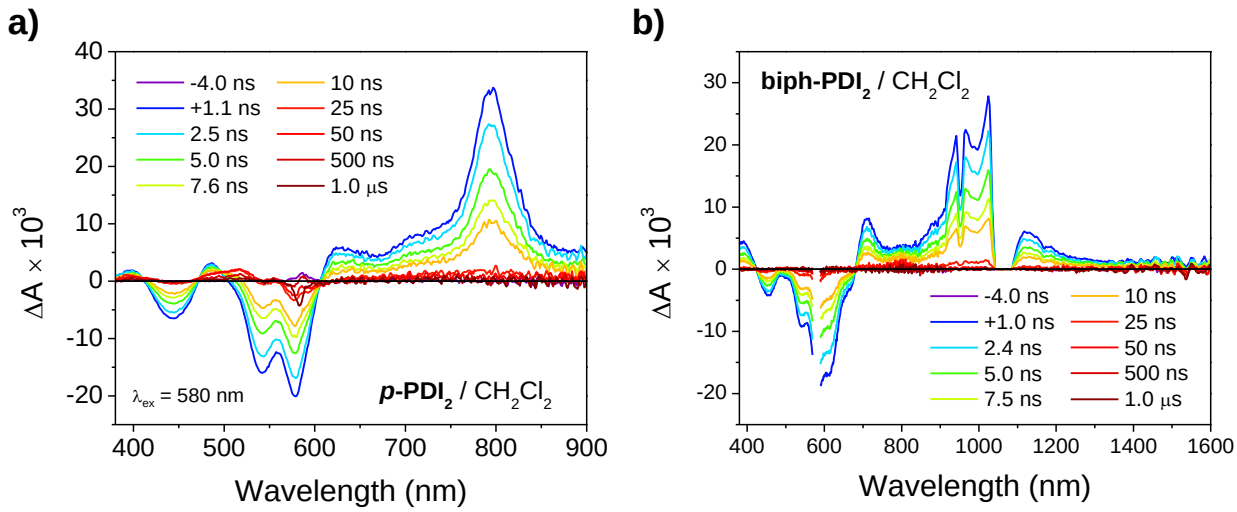


**Figure S21.** nsTA spectra of a) ***p*-PDI$_2$**, and **biph-PDI$_2$** in $CH_2Cl_2$ following $\lambda_{ex}$ = 580 nm excitation (1.0 μJ/pulse, ~120 fs) at 298 K. Scatter of the supercontinuum probe fundamental near 1064 nm is suppressed for clarity.

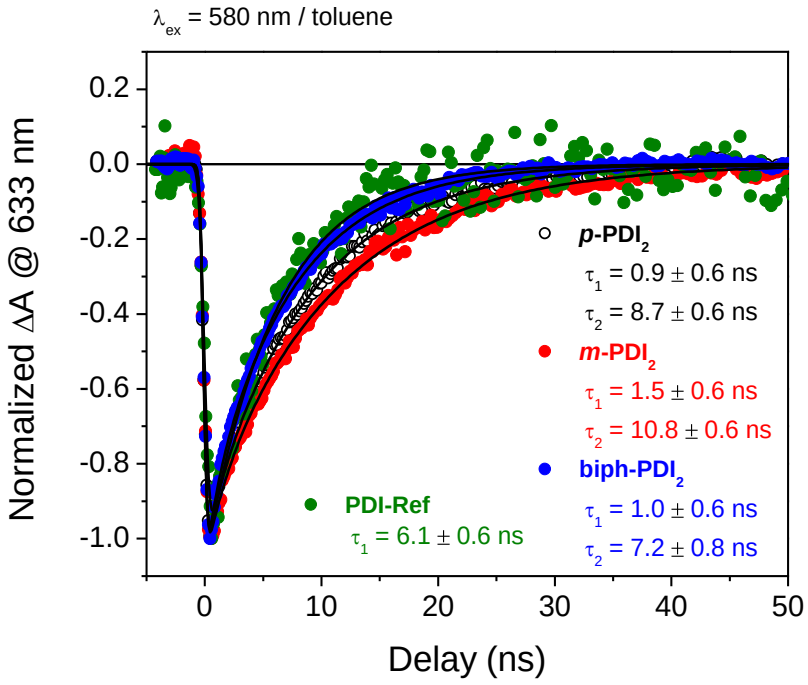


**Figure S22.** Single-wavelength kinetic fits to the nsTA data in toluene at 633 nm ($S_0$ bleach).

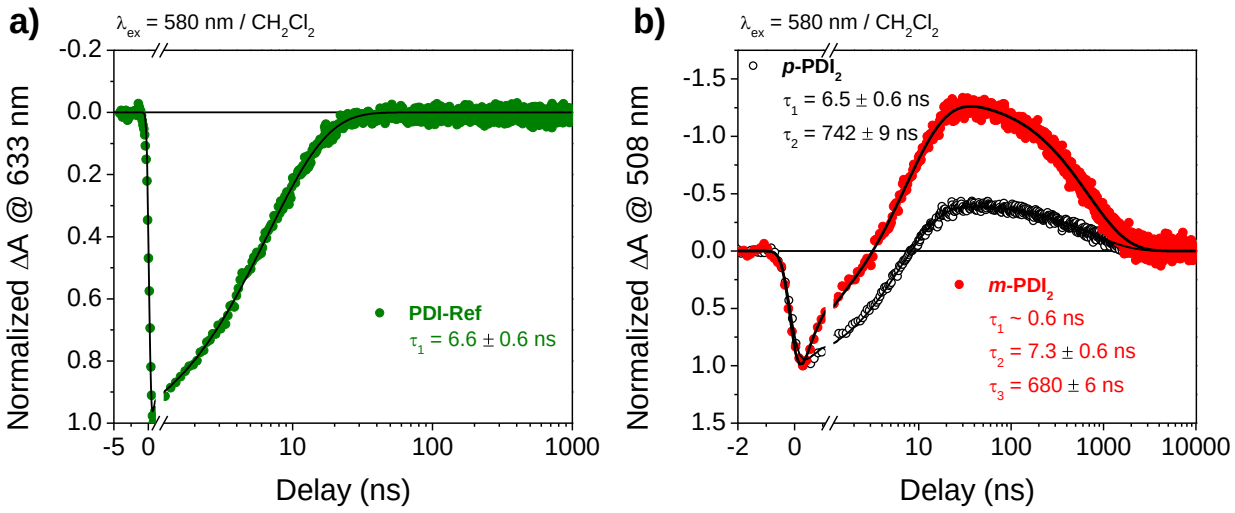


**Figure S23.** Single-wavelength kinetic fits to the nsTA data in $CH_2Cl_2$ at a) 633 nm ($S_0$ bleach) for **PDI-Ref** and **biph-PDI$_2$**, and b) 508 nm ($S_0$ bleach and $T_1$ absorption) for ***p*-PDI$_2$** and ***m*-PDI$_2$.**

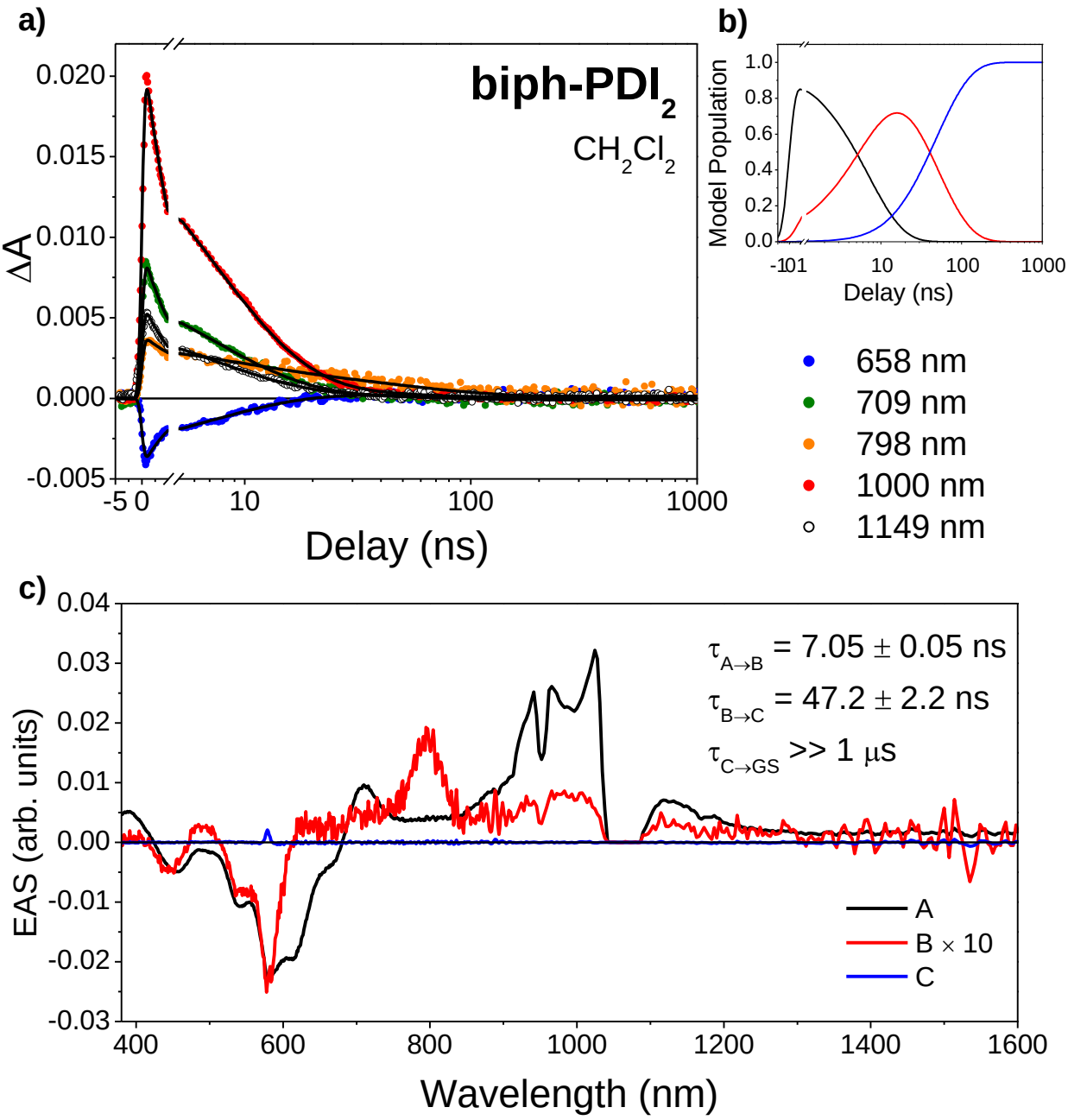


**Figure S24.** a) Global fits to selected nsTA wavelengths in **biph-PDI₂** ($\lambda_{ex}$ = 580 nm) in $CH_2Cl_2$ to a sequential A → B → C → ground state kinetic model. Fits are shown as solid lines. b) Solution to the kinetic model using the fit parameters. C) Evolution-associated spectra obtained from deconvolution of the data set with the kinetic fit solution. State A represents the $S_1$ state, state B is the SB-CS state, and state C represents the $T_1$ state. Scatter of the supercontinuum probe fundamental near 1064 nm is suppressed for clarity.

*c. fs Fluorescence Up-Conversion Spectroscopy*

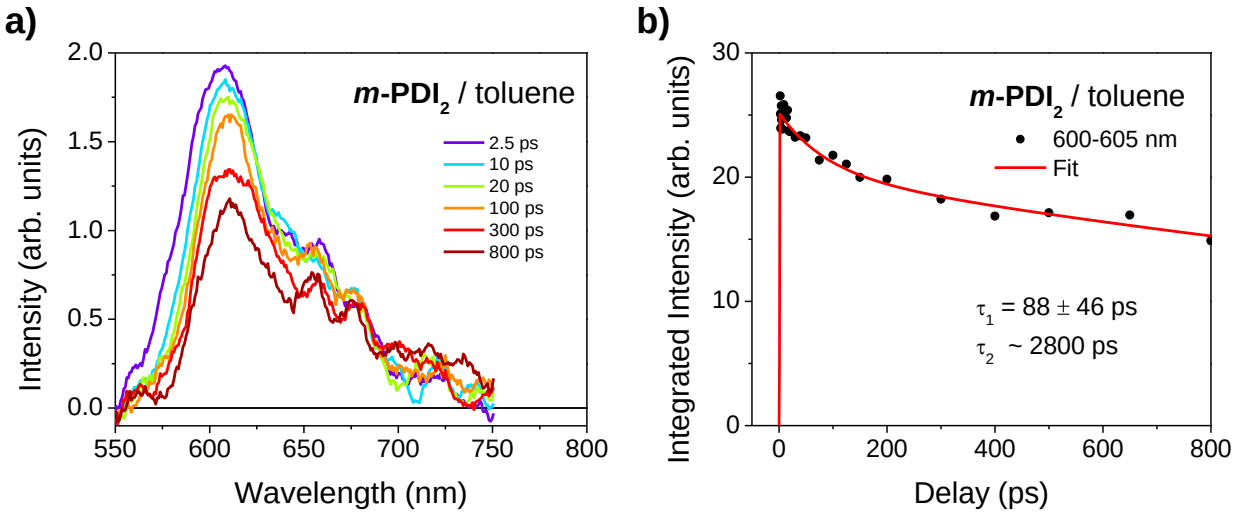


**Figure S25.** a) fs fluorescence up-conversion spectra for ***m*-PDI$_2$** in toluene following 580 nm excitation (300 nJ/pulse). b) Single-wavelength kinetic fit to the integrated intensity between 585-645 nm. The longer time constant is limited by the short travel length of translation stage (< 2 ns) in the up-conversion experiment.

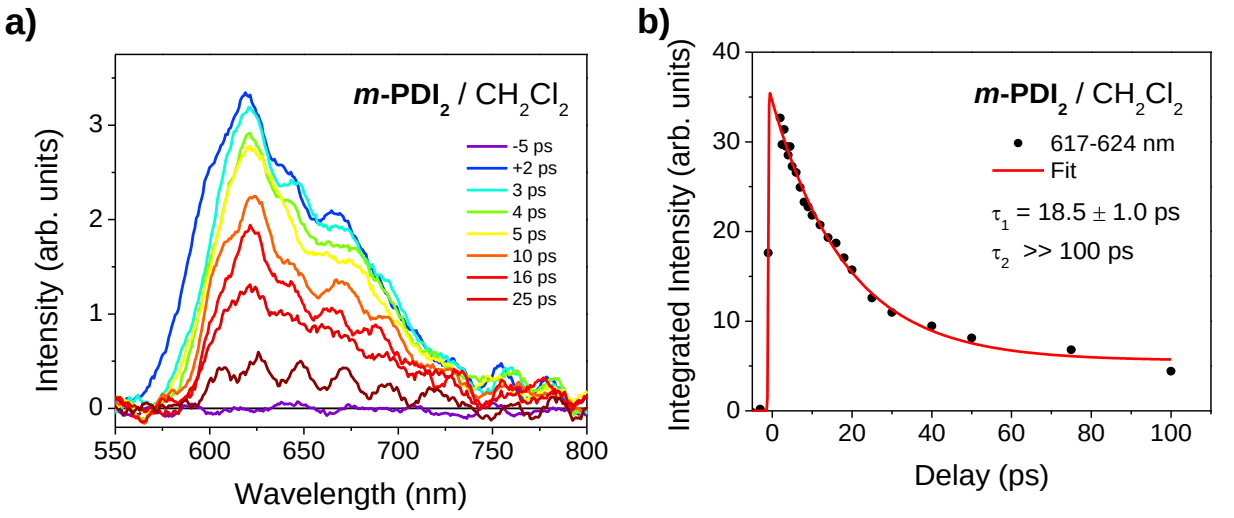


**Figure S26.** a) fs fluorescence up-conversion spectra for ***m*-PDI$_2$** in $CH_2Cl_2$ following 580 nm excitation (300 nJ/pulse). b) Single-wavelength kinetic fit to the integrated intensity between 617-624 nm.

*d. psTRF Spectroscopy*

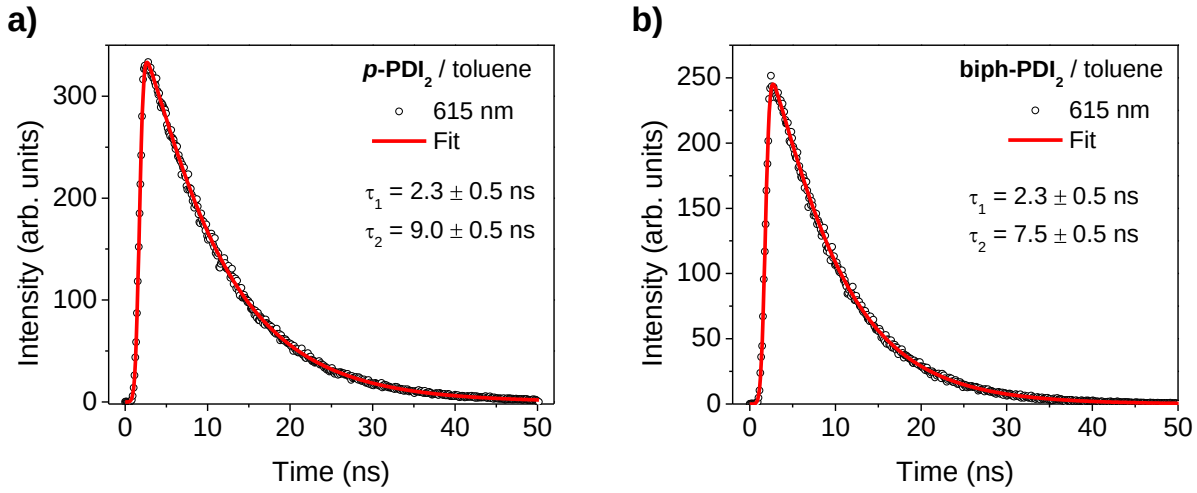


**Figure S27.** Single-wavelength kinetic fits to the psTRF data for a) ***p*-PDI$_2$** and b) **biph-PDI$_2$** in toluene for the 50 ns window fit with a bi-exponential decay.

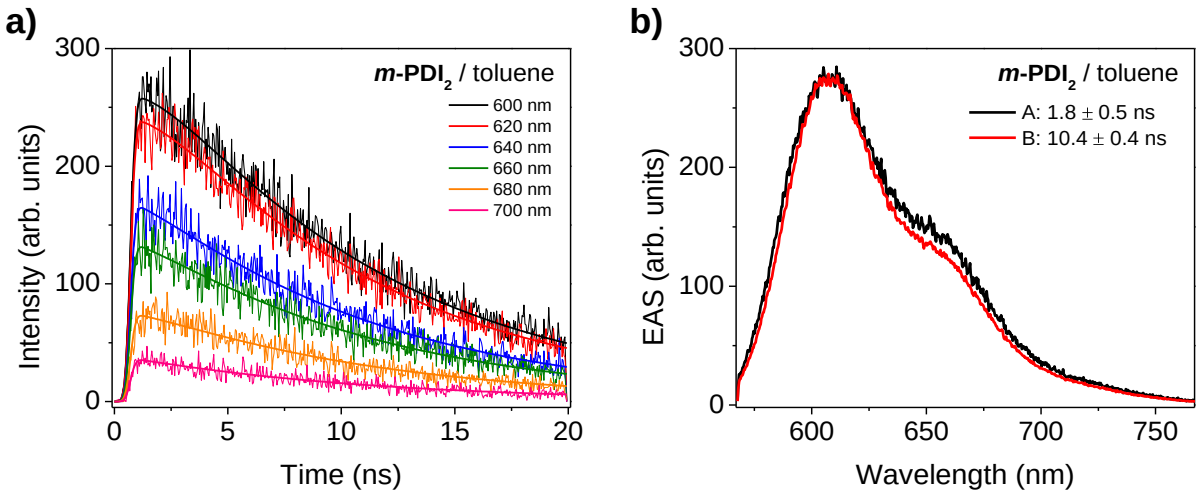


**Figure S28.** a) Global analysis of the psTRF data for ***m*-PDI$_2$** in toluene for the 20 ns window. a) Kinetic fits to a sequential A → B → ground state model, and b) evolution-associated psTRF spectra (EAS) showing no spectral shifting.

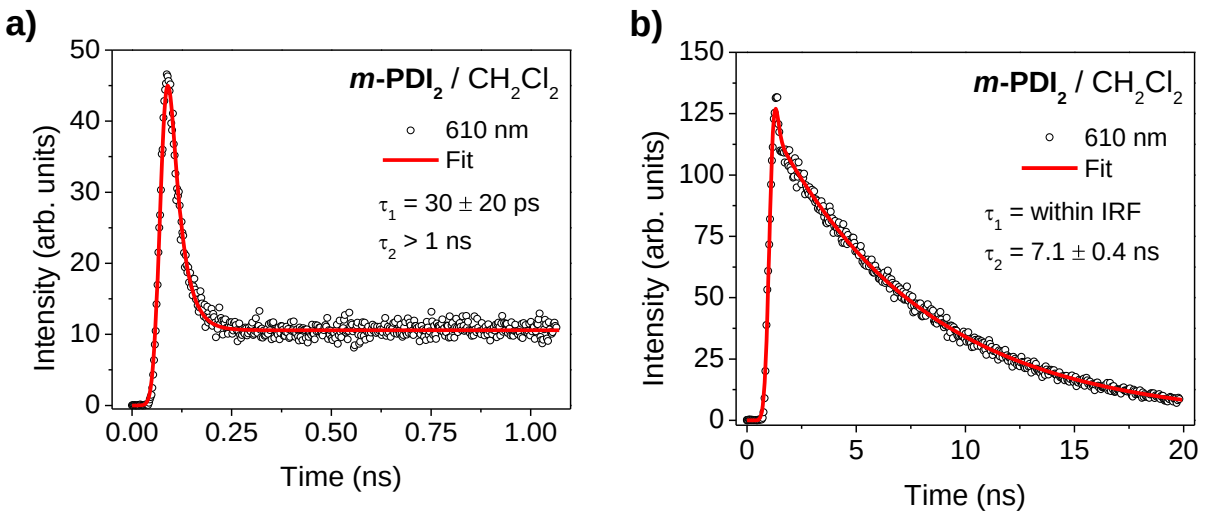


**Figure S29.** Single-wavelength kinetic fits to the psTRF data for ***m*-PDI₂** in $CH_2Cl_2$ for the a) 1 ns and b) 20 ns windows fit with a bi-exponential decay.

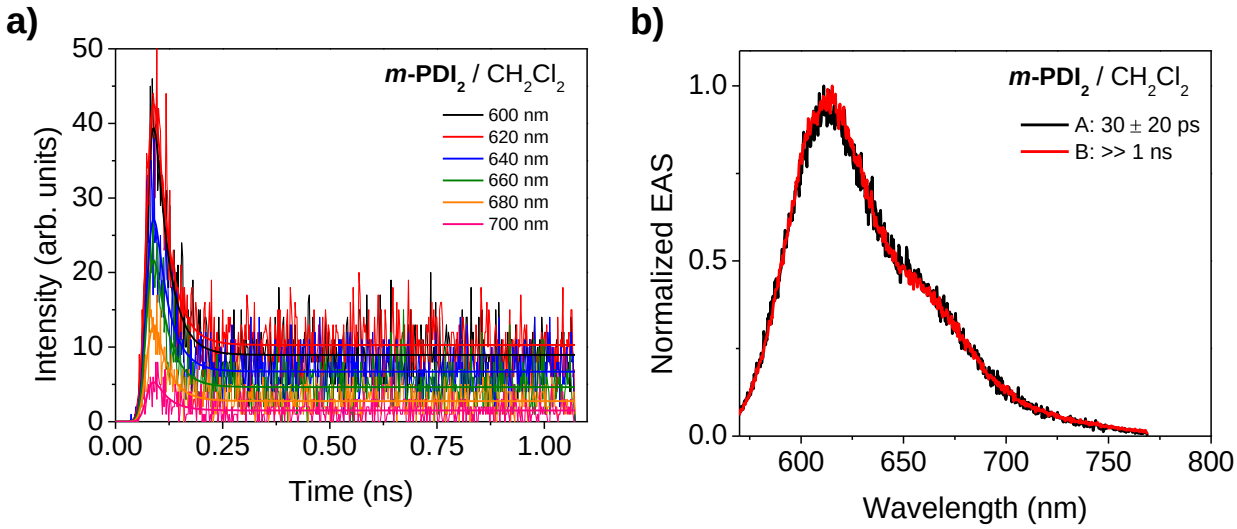


**Figure S30.** Global analysis of the psTRF data for ***m*-PDI₂** in $CH_2Cl_2$ for the 1 ns window. a) Kinetic fits to a sequential A → B → ground state model, and b) normalized evolution-associated psTRF spectra (EAS) showing no spectral evolution.

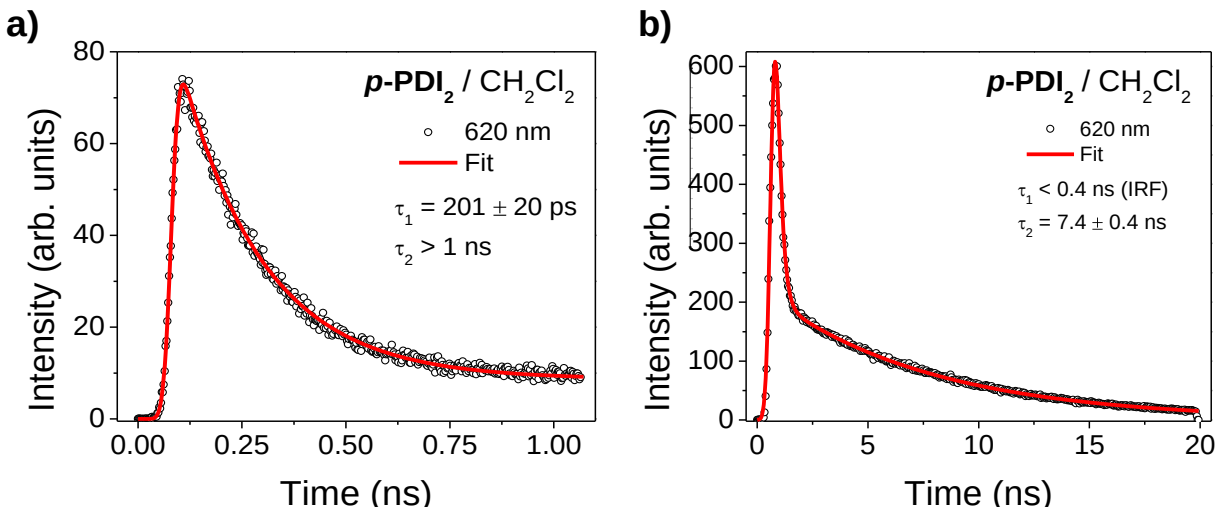


**Figure S31.** Single-wavelength kinetic fits to the psTRF data for ***p*-PDI$_2$** in $CH_2Cl_2$ for the a) 1 ns and b) 20 ns windows fit with a bi-exponential decay.

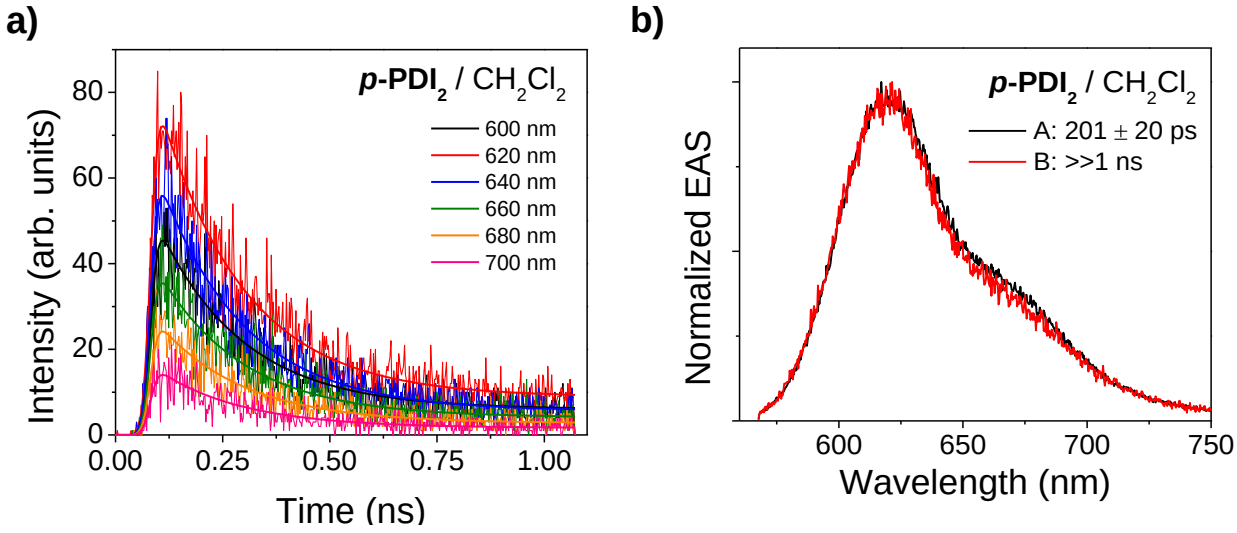


**Figure S32.** a) Global analysis of the psTRF data for ***p*-PDI$_2$** in $CH_2Cl_2$ for the 1 ns window. a) Kinetic fits to a sequential A → B → ground state model, and b) normalized evolution-associated psTRF spectra (EAS) showing no spectral evolution.

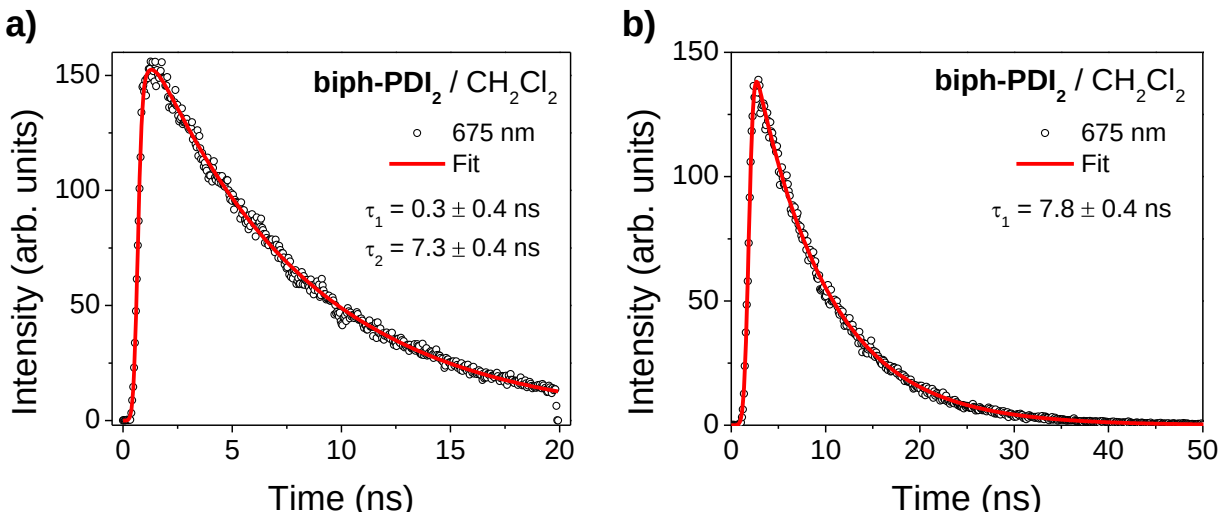


**Figure S33.** Single-wavelength kinetic fits to the psTRF data for **biph-PDI₂** in $CH_2Cl_2$ for the a) 1 ns windows fit with a bi-exponential decay and b) 20 ns windows fit with a single exponential decay.

*e. fsIR Spectroscopy*

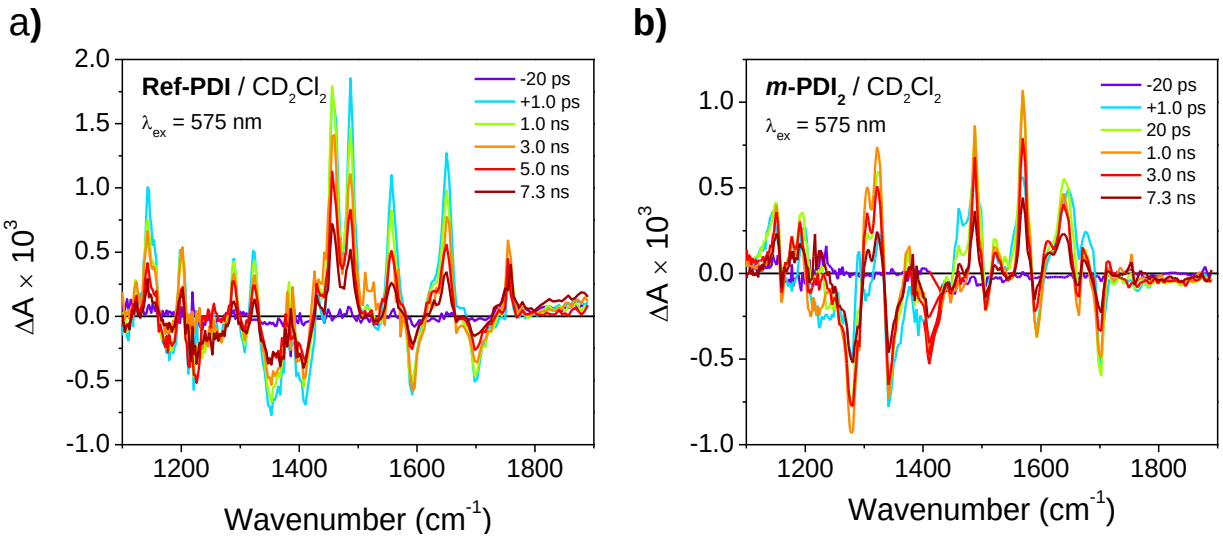


**Figure S34.** fsIR spectra of a) **PDI-Ref**, b) ***m*-PDI$_2$** in $CD_2Cl_2$ following $\lambda_{ex}$ = 575 nm excitation (1-2 μJ/pulse, ~120 fs) at 298 K.

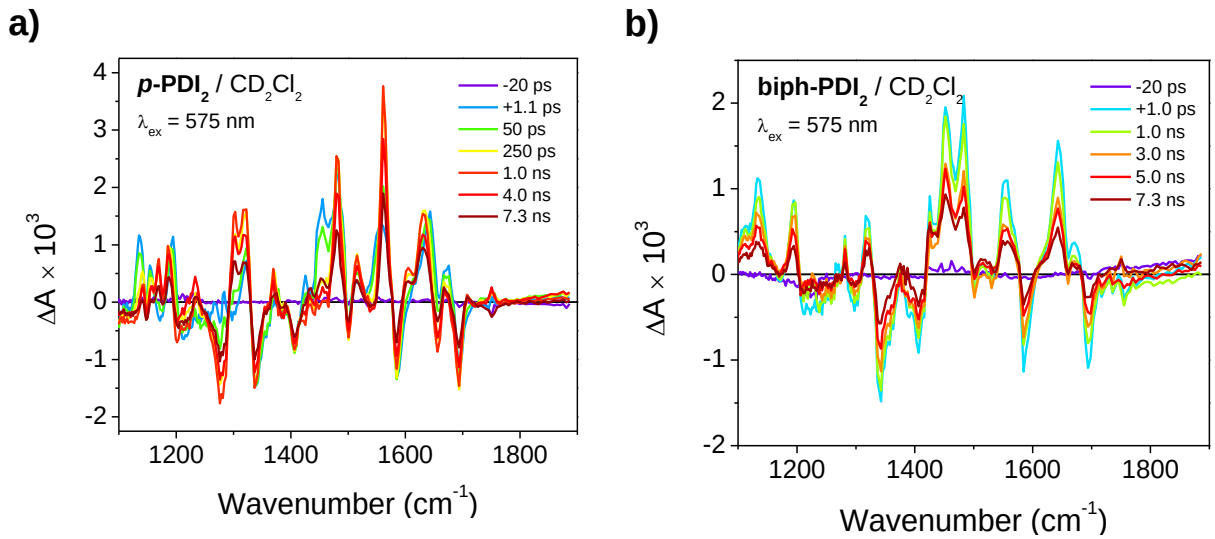


**Figure S35.** fsIR spectra of a) ***p*-PDI$_2$**, and b) **biph-PDI$_2$** in $CD_2Cl_2$ following $\lambda_{ex}$ = 575 nm excitation (1-2 μJ/pulse, ~120 fs) at 298 K.

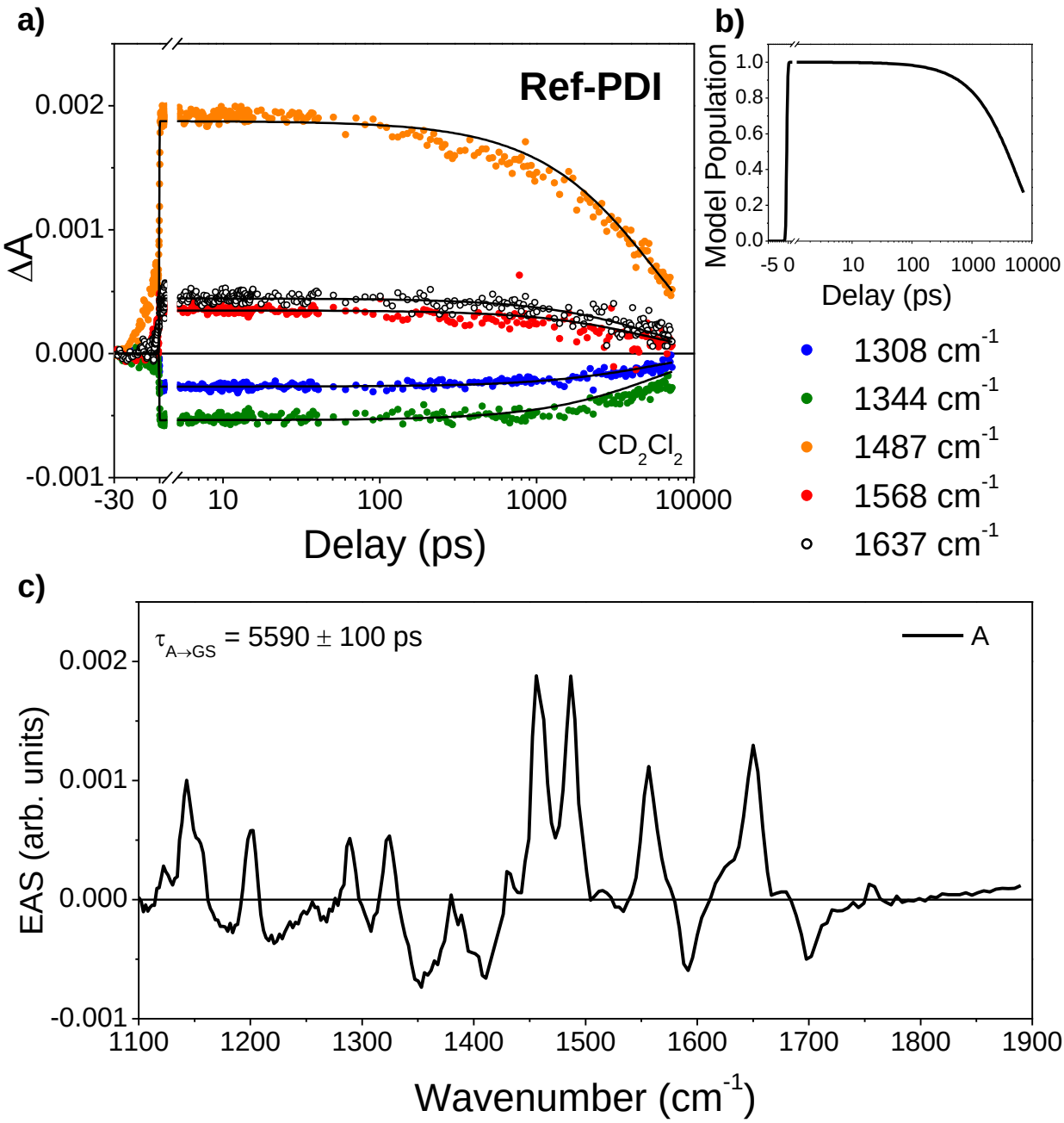


**Figure S36.** a) Global fits to selected fsIR frequencies in **PDI-Ref** ($\lambda_{ex}$ = 575 nm) to a sequential A → ground state kinetic model. Fits are shown as solid lines and fitted time constants are shown. b) Solution to the kinetic model using the fit parameters. C) Evolution-associated spectra obtained from deconvolution of the data set with the kinetic fit solution. State A represents the $S_1$ state.

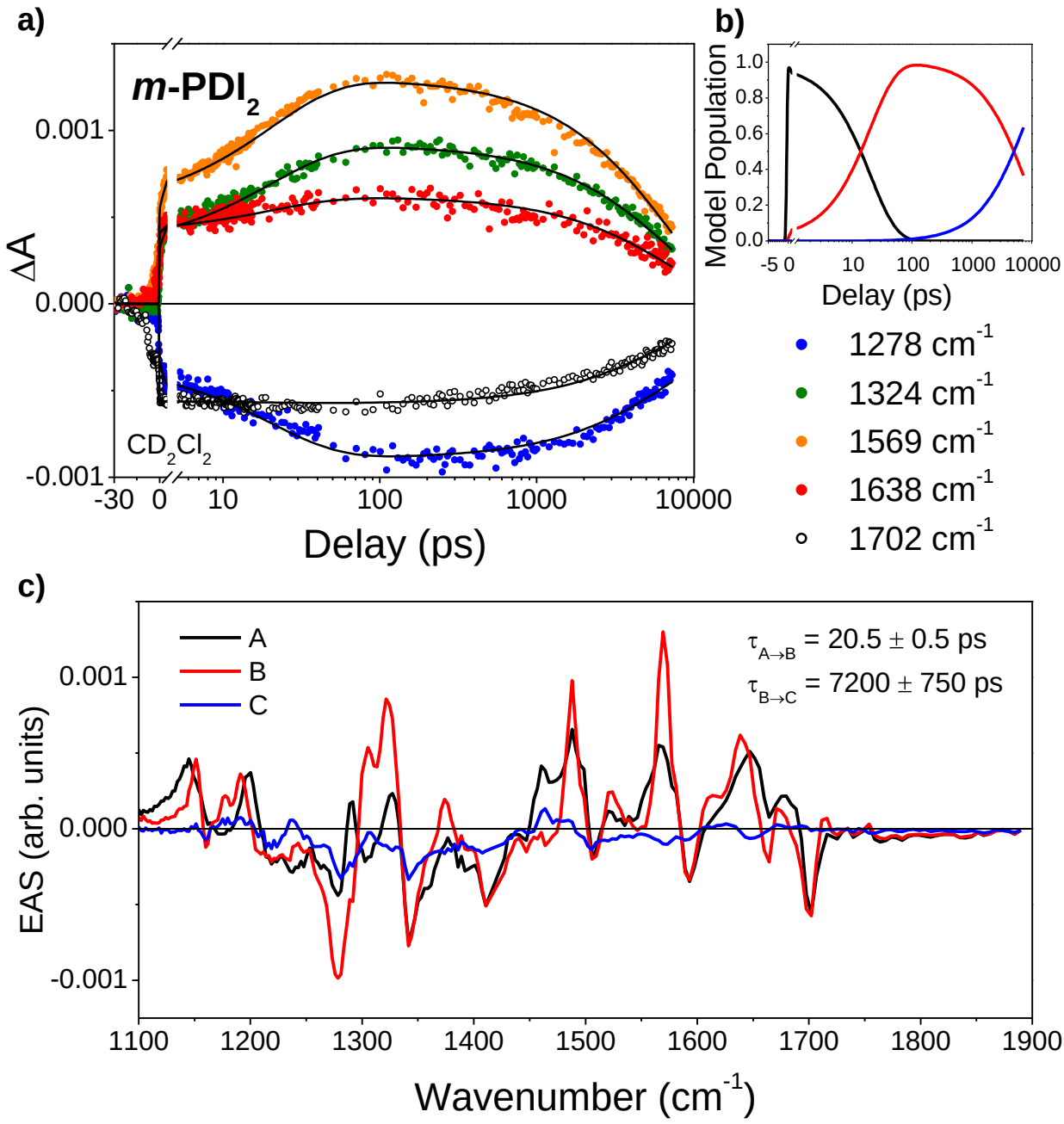


**Figure S37.** a) Global fits to selected fsIR frequencies in ***m*-PDI₂** ($\lambda_{ex}$ = 575 nm) to a sequential A → B → C kinetic model described in the text. Fits are shown as solid lines and fitted time constants are shown. b) Solution to the kinetic model using the fit parameters. c) Evolution-associated spectra obtained from deconvolution of the data set with the kinetic fit solution. State A represents the $S_1$ state, B represents the SB-CS state, and C is the $T_1$ state of ***m*-PDI₂**.

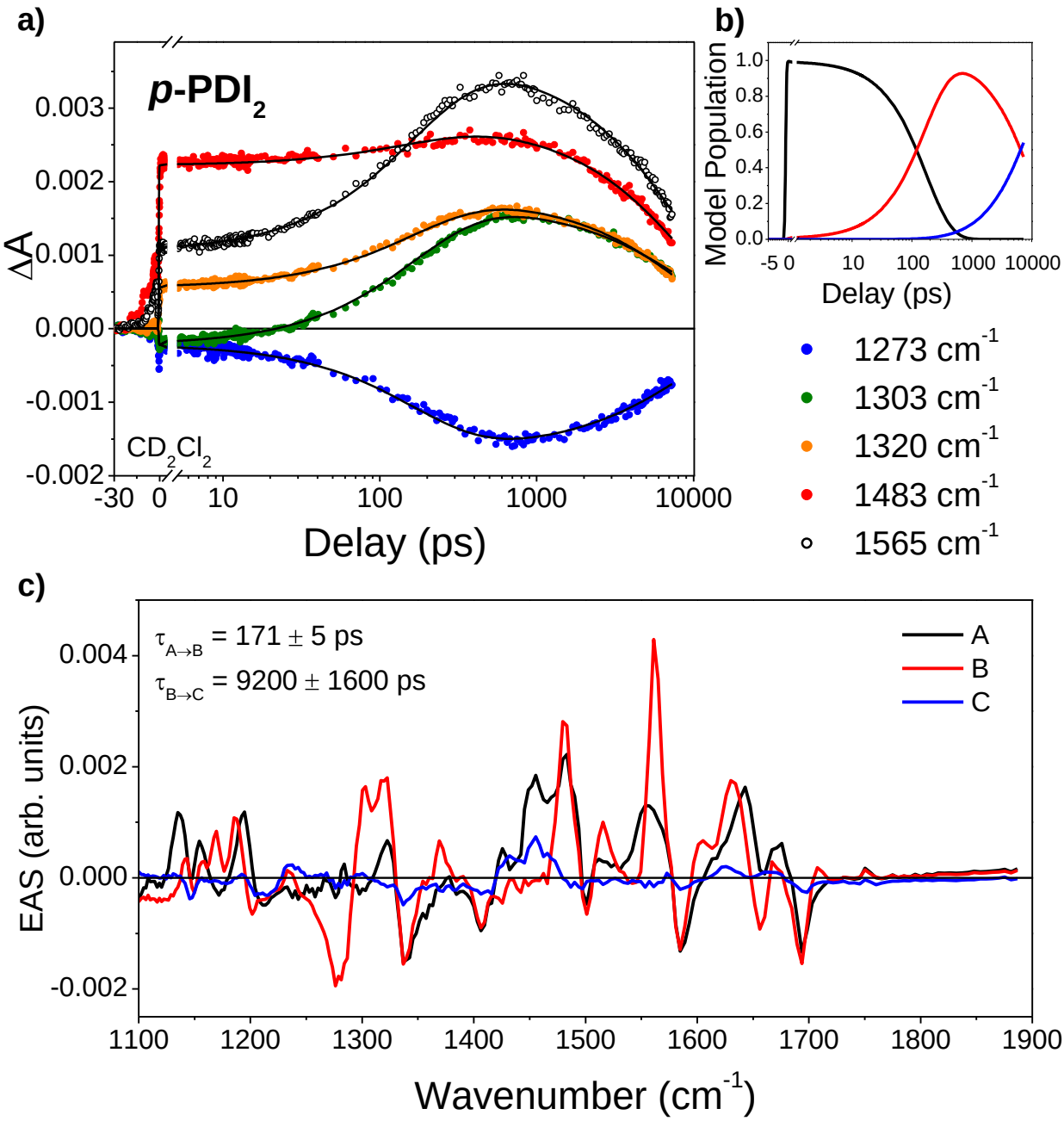


**Figure S38.** a) Global fits to selected fsIR frequencies in ***p*-PDI₂** ($\lambda_{ex}$ = 575 nm) to a sequential A → B → C kinetic model described in the text. Fits are shown as solid lines and fitted time constants are shown. b) Solution to the kinetic model using the fit parameters. c) Evolution-associated spectra obtained from deconvolution of the data set with the kinetic fit solution. State A represents the $S_1$ state, B represents the SB-CS state, and C is the $T_1$ state of ***p*-PDI₂**.

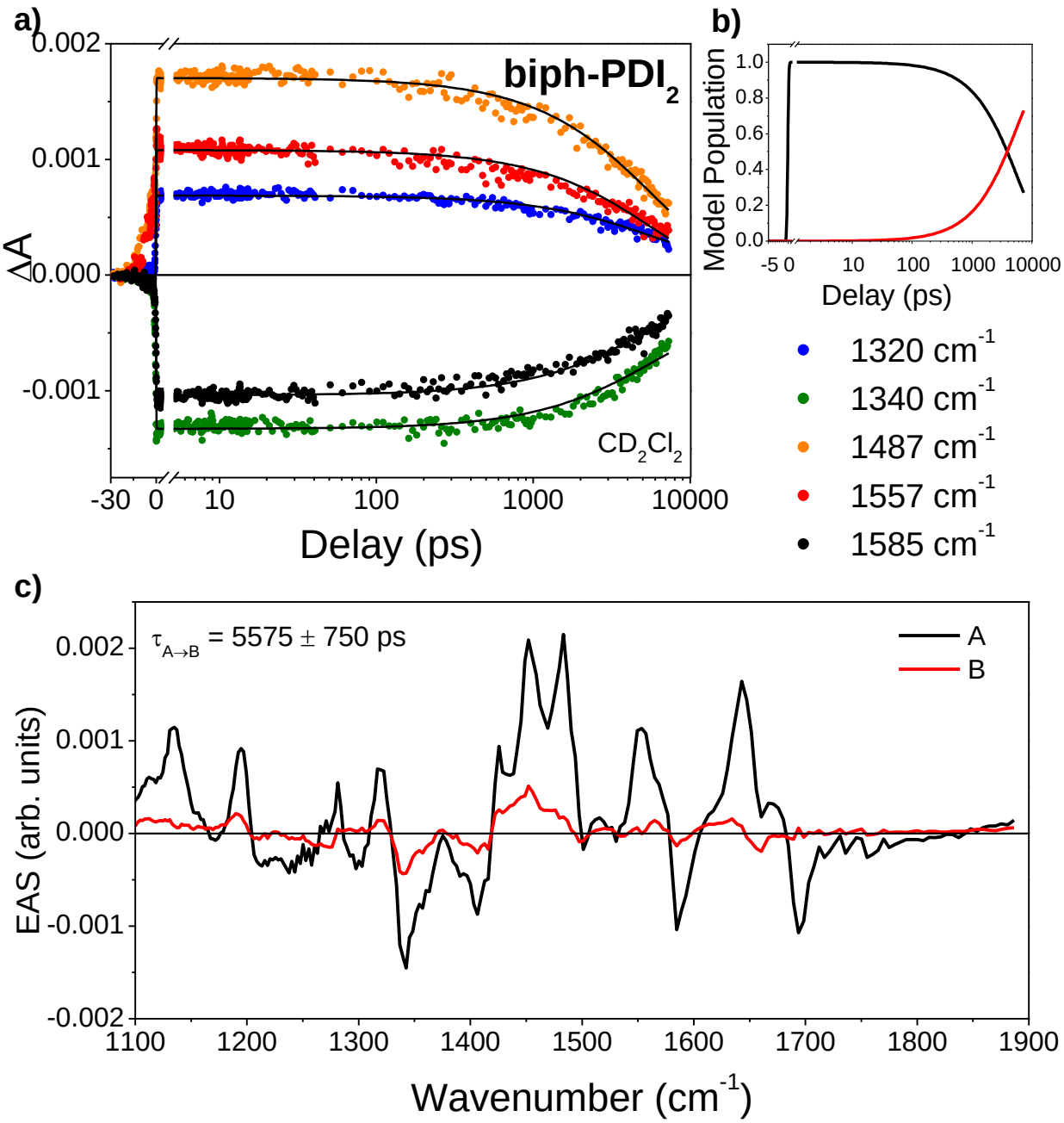


**Figure S39.** a) Global fits to selected fsIR frequencies in **biph-PDI$_2$** ($\lambda_{ex}$ = 575 nm) to a sequential A → B kinetic model. Fits are shown as solid lines and fitted time constants are shown. b) Solution to the kinetic model using the fit parameters. c) Evolution-associated spectra obtained from deconvolution of the data set with the kinetic fit solution. State A represents the $S_1$ state, and B shows indications of SB-CS (see below).

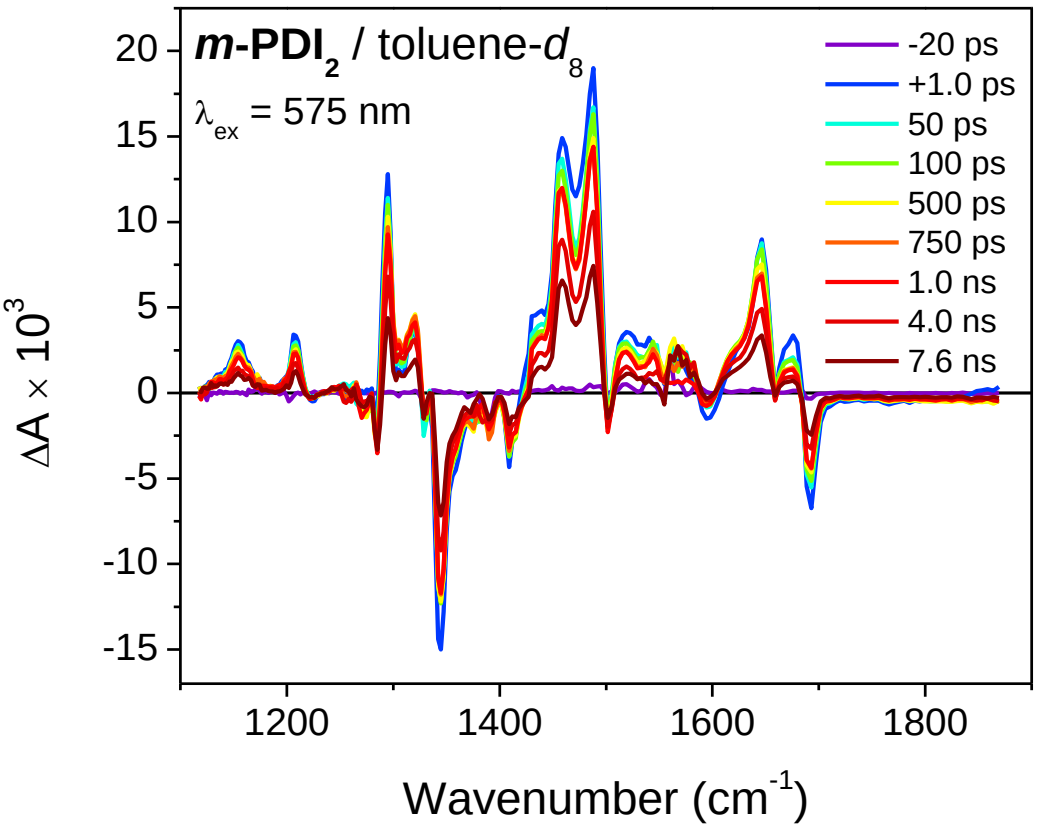


**Figure S40.** fsIR spectra of ***m*-PDI$_2$** in toluene-$d_8$ following $\lambda_{ex}$ = 575 nm excitation (2 μJ/pulse, ~120 fs) at 298 K.

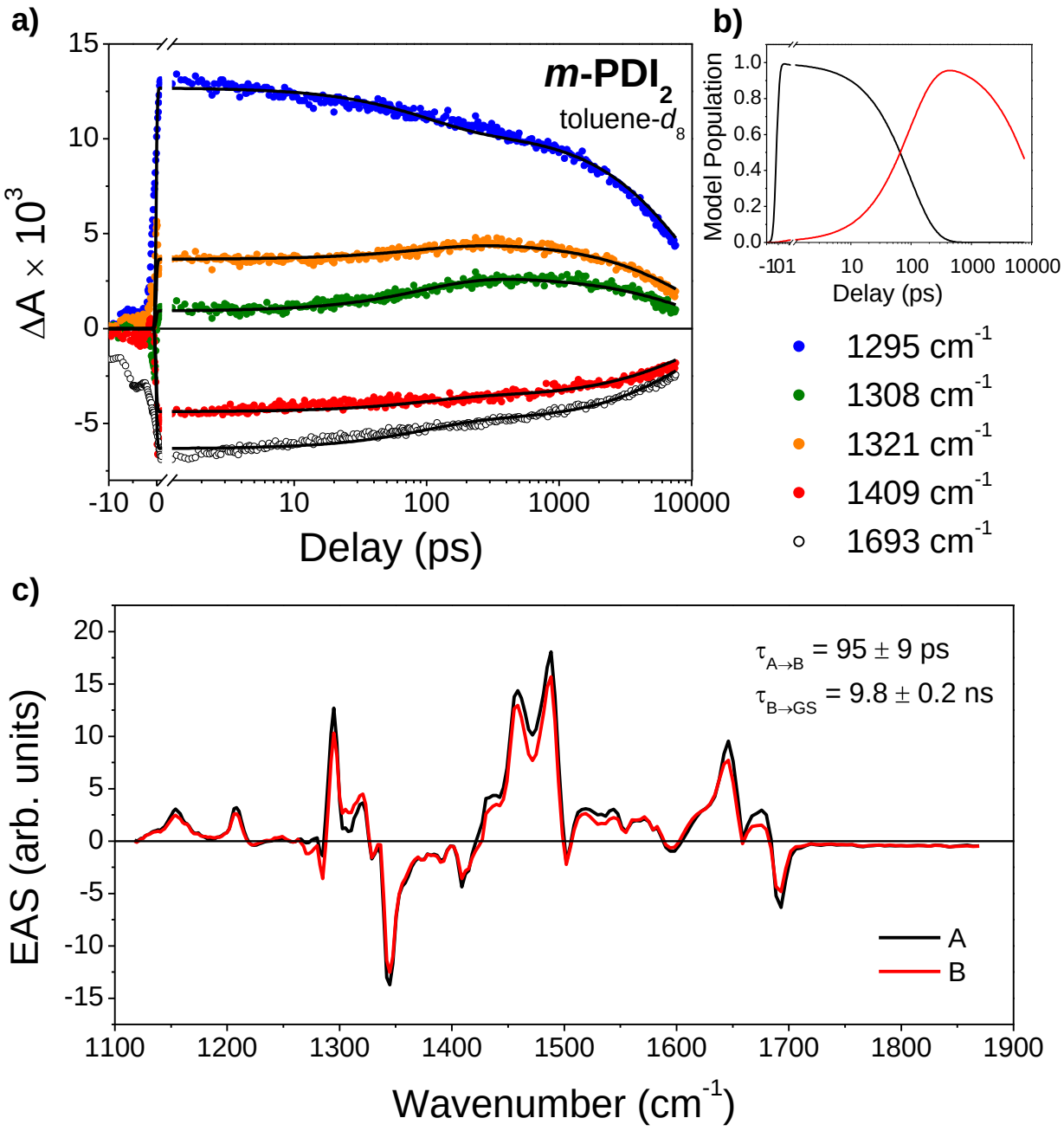


**Figure S41.** a) Global fits to selected fsIR frequencies in ***m*-PDI$_2$** ($\lambda_{ex}$ = 575 nm) in toluene-$d_8$ to a sequential A → B → ground state kinetic model. Fits are shown as solid lines and fitted time constants are shown. b) Solution to the kinetic model using the fit parameters. c) Evolution-associated spectra obtained from deconvolution of the data set with the kinetic fit solution. State A represents the $S_1$ state, and B shows indications of SB-CS (see below).

*f. nsIR Spectroscopy*

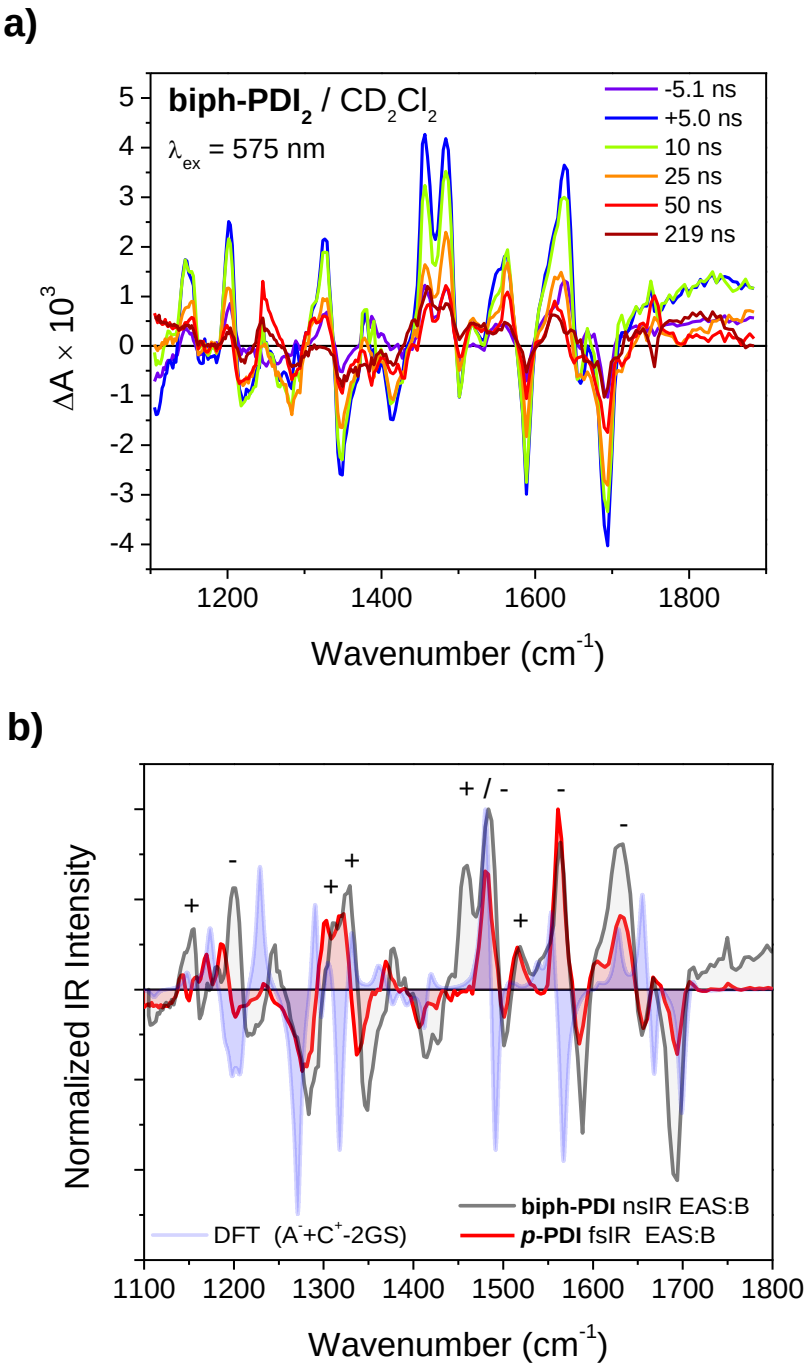


**Figure S42.** a) nsIR spectra of **biph-PDI$_2$** in $CD_2Cl_2$ following 575 nm (5 μJ/pulse), 3 ns excitation. b) Overlay of the second evolution-associated spectra (EAS:B) for the nsIR data of **biph-PDI$_2$** (gray), and the fsIR data of ***p*-PDI$_2$** (red) in $CD_2Cl_2$, with the DFT-calculated transient IR spectrum (blue) supporting the assignment of SB-CS for the ~50 ns-lived component. The simulated spectrum is the sum of the computed anion ($A^{-\bullet}$) and cation ($C^{+\bullet}$) spectra minus twice the ground state spectrum: $A^{-\bullet} + C^{+\bullet} - 2GS$. See below for computational details. Anion and cation features are labeled (-) and (+), respectively.

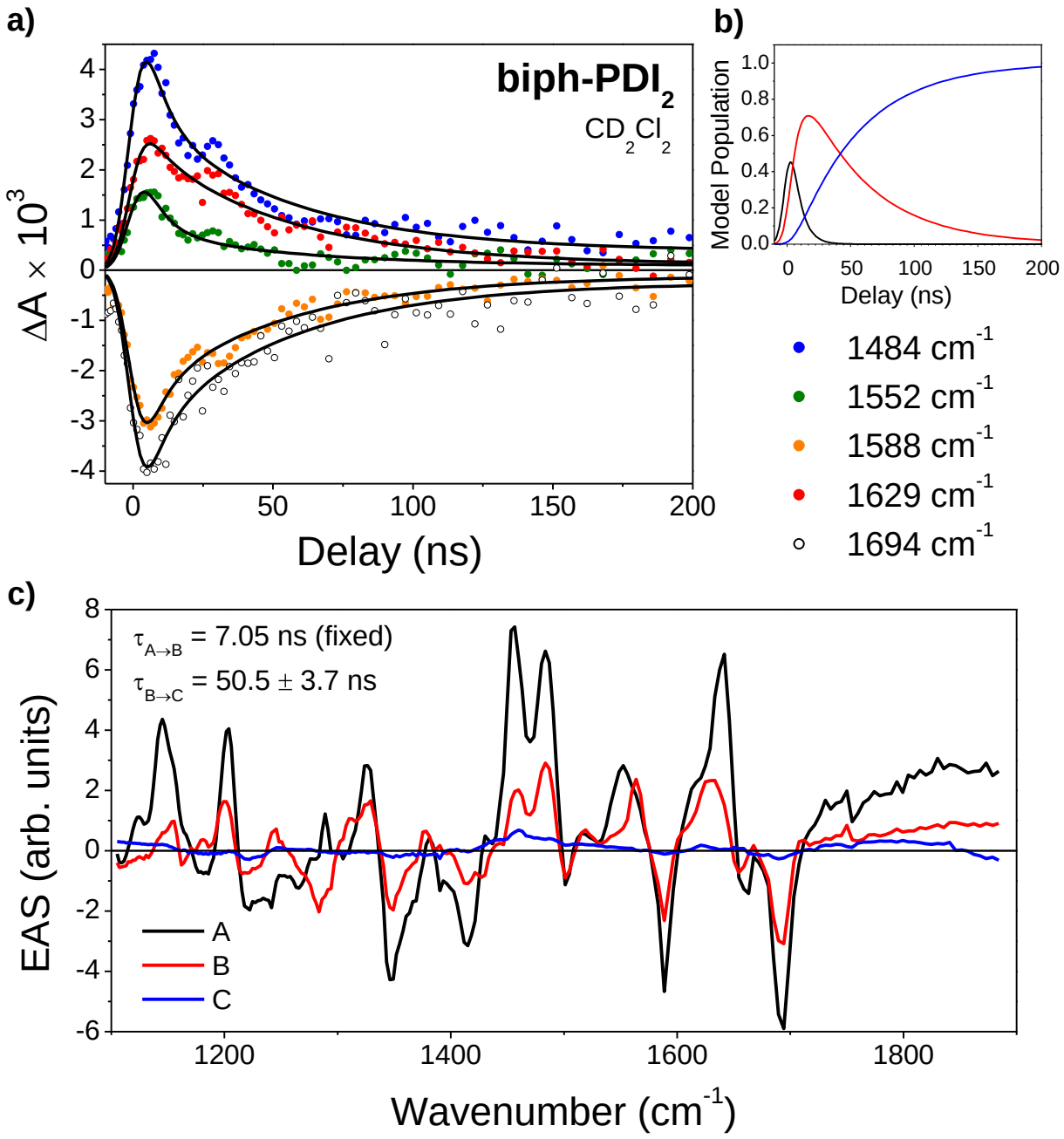


**Figure S43.** a) Global fits to selected nsIR frequencies in **biph-PDI₂** ($\lambda_{ex}$ = 575 nm) in $CD_2Cl_2$ to a sequential A → B → C kinetic model described in the text. Fits are shown as solid lines and fitted time constants are shown. b) Solution to the kinetic model using the fit parameters. c) Evolution-associated spectra obtained from deconvolution of the data set with the kinetic fit solution. State A represents the $S_1$ state, B represents the SB-CS state, and C is the $T_1$ state of **biph-PDI₂**.

## 5. Kinetic Analysis

The effective observed rates ($\lambda_i$) for the monomer and dimers were determined by fitting the data to a sequential model as discussed above. These values and the fluorescence quantum yields ($\Phi_f$) for the monomer **PDI-Ref** are given in Table S1, and those for the dimers are given in Table 2.

**Table S1**. Simplified kinetic parameters for **PDI-Ref** taken from nsTA measurements in toluene and $CH_2Cl_2$. Fast relaxation (<ns) are ignored given the high fluorescence quantum yields.

| | **PDI-Ref** | |
|---|---|---|
| | Toluene | $CH_2Cl_2$ |
| $\lambda_0$ | $(6.10\ ns)^{-1}$ | $(6.40\ ns)^{-1}$ |
| $k_f$ | $(6.10\ ns)^{-1}$ | $(7.05\ ns)^{-1}$ |
| $k_0$ | ~0 | $(69.6\ ns)^{-1}$ |
| $\Phi_f$ | 0.95 | 0.91 |

*Monomer Kinetics.* The $S_1$ state can decay non-radiatively and fluorescence with rates $k_0$ and $k_f$, respectively. These rates can be estimated from the analogous processes in the **PDI-Ref** monomer reference compound: $k_f = \lambda_0\phi_0$, and $k_0 = \lambda_0(1-\phi_0)$, where $\phi_0$ and $\lambda_0$ are the measured fluorescence quantum yield and observed decay rate of the monomer. No triplet formation is observed in the monomer and so is neglected. The values of $k_f$ and $k_0$ are also given in Table S1.

*Reversible SB-CS.* The general case of the equilibrium between the fluorescent $S_1$ and SB-CS states with a triplet recombination pathway shown in Figure S45 can be modeled using the first-order rate matrix $\boldsymbol{M}$ below in equation S2.

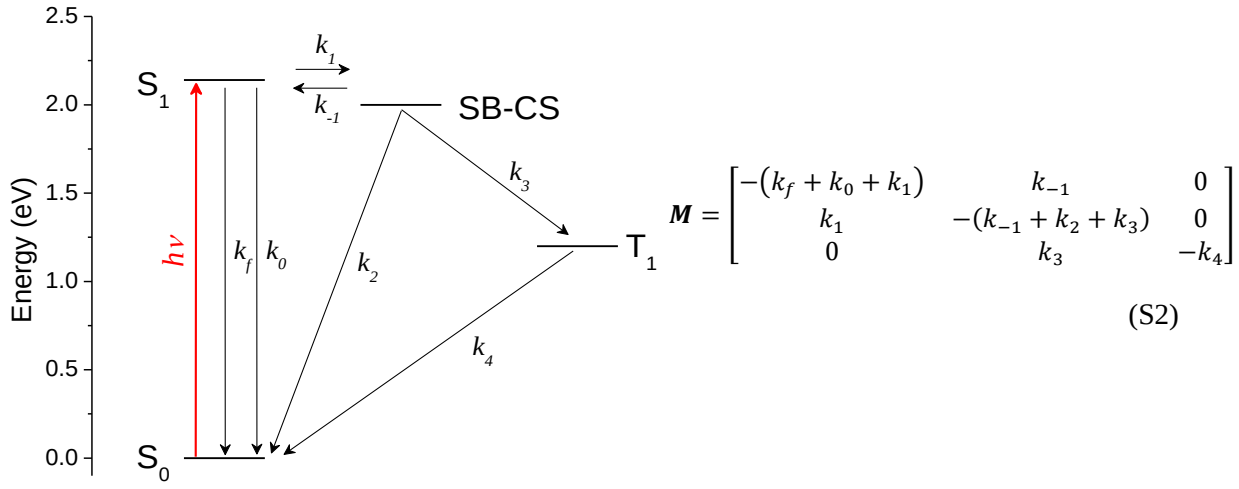


$$\boldsymbol{M} = \begin{bmatrix} -(k_f + k_0 + k_1) & k_{-1} & 0 \\ k_1 & -(k_{-1} + k_2 + k_3) & 0 \\ 0 & k_3 & -k_4 \end{bmatrix} \quad \text{(S2)}$$

**Figure S45.** Energy level diagram describing equilibrium between $S_1$ and SB-CS states and rate matrix.

The eigenvalues for this matrix are:

$$\lambda_{1,2} = \frac{1}{2}\left(k_f + k_0 + k_1 + k_{-1} + k_2 + k_3\right) \pm \frac{1}{2}\sqrt{\left(k_f + k_0 + k_1 + k_{-1} + k_2 + k_3\right)^2 - 4\left[\left(k_f + k_0 + k_1\right)\left(k_{-1} + k_2 + k_3\right) - k_1 k_{-1}\right]} \quad \text{(S3a)}$$

$$\lambda_3 = k_4 \quad \text{(S3b)}$$

Identification of $k_4$ as the slowest rate from the nsTA data is straightforward, as it is not involved in the reversible process; however, extraction of $k_1$, $k_{-1}$, $k_2$, and $k_3$ requires additional information from external experiments. This can be accomplished using the measured fluorescence and triplet yields of the dimers $\phi_f$ and $\phi_T$.

*Calculation of Quantum Yields $\Phi_f$ and $\Phi_T$.* Since the equilibrium enables a pathway for delayed emission, the contributions from fluorescence following charge recombination to the excited state must be considered. We will model each event in the SB-CS process as a random walk with the probability for each step *i* given as $k_i/\Sigma k_i$ shown in Figure S45. The random walk leads to successive fluorescence events as the reverse

transfer repopulates the excited state following SB-CS, leading to an infinite series which converges to give:

$$\Phi_f = \frac{k_f(k_{-1} + k_2 + k_3)}{\big(k_f + k_0 + k_1\big)(k_{-1} + k_2 + k_3) - k_1 k_{-1}} \tag{S4a}$$

We can obtain a similar expression for the triplet yield:

$$\Phi_T = \frac{k_1 k_3}{\big(k_f + k_0 + k_1\big)(k_{-1} + k_2 + k_3) - k_1 k_{-1}} \tag{S4b}$$

*Evaluation of Rate Constants.* The quantum yield equations along with eq S3 give a fully determined system to extract each rate constant:

$$k_1 = \lambda_1 + \lambda_2 - \left(\frac{\Phi_f}{k_f}\right)\lambda_1\lambda_2 - k_f - k_0 \tag{S5a}$$

$$k_{-1} = \frac{\lambda_1\lambda_2}{k_1}\left(\frac{\Phi_f}{k_f}\right)\left[\left(1 - \frac{1}{\phi_f}\right)k_f + k_0 + k_1\right] \tag{S5b}$$

$$k_2 = \lambda_1\lambda_2\left(\frac{\Phi_f}{k_f} - \frac{\Phi_T}{k_1}\right) - k_{-1} \tag{S5c}$$

$$k_3 = \lambda_1\lambda_2\left(\frac{\Phi_T}{k_1}\right) \tag{S5d}$$

Values for these rate constants are given in Table 3 in the main text. The ~ns time constants are taken from the nsTA or psTRF data since they will be more reliable than the fsTA-extracted values when the time constants approach the ~8 ns delay window.

The forward and reverse SB-CS rate constants can then be used to determine the equilibrium constant $K$ and the driving force for SB-CS are given by:

$$K = \frac{k_1}{k_{-1}} \tag{S6a}$$

$$\Delta G_{CS} = -k_B T \ln K = -k_B T \ln\left(\frac{k_1}{k_{-1}}\right) \tag{S6b}$$

We can also compute the values for $\Phi_{f,p}$ and $\Phi_{f,d}$, as given in Table 3.

$$\Phi_{f,p} = \frac{k_f}{k_f + k_0 + k_1} \tag{S7a}$$

$$\Phi_{f,d} = \left(\frac{k_1 k_{-1}}{\lambda_1 \lambda_2}\right)\left(\frac{k_f}{k_f + k_0 + k_1}\right) = \left(\frac{k_1 k_{-1}}{\lambda_1 \lambda_2}\right)\Phi_{f,p}$$

$$= \Phi_{f,p}\left(\frac{\phi_f}{k_f}\right)\left[\left(1 - \frac{1}{\phi_f}\right)k_f + k_0 + k_1\right] \tag{S7b}$$

We assume again that the triplet yields are zero. However, this approximation will only affect the how the values of $k_2$ and $k_3$ are partitioned; the sum $k_2 + k_2$ remains constant. Thus, this assumption does not impact the equilibrium constant or values derived from it. This assumption also necessitates $k_4 = 0$, which contradicts the nsTA data, but that rate constant is also not involved in the equilibrium. This analysis also suggests that the majority of the emission in these dimers is delayed.

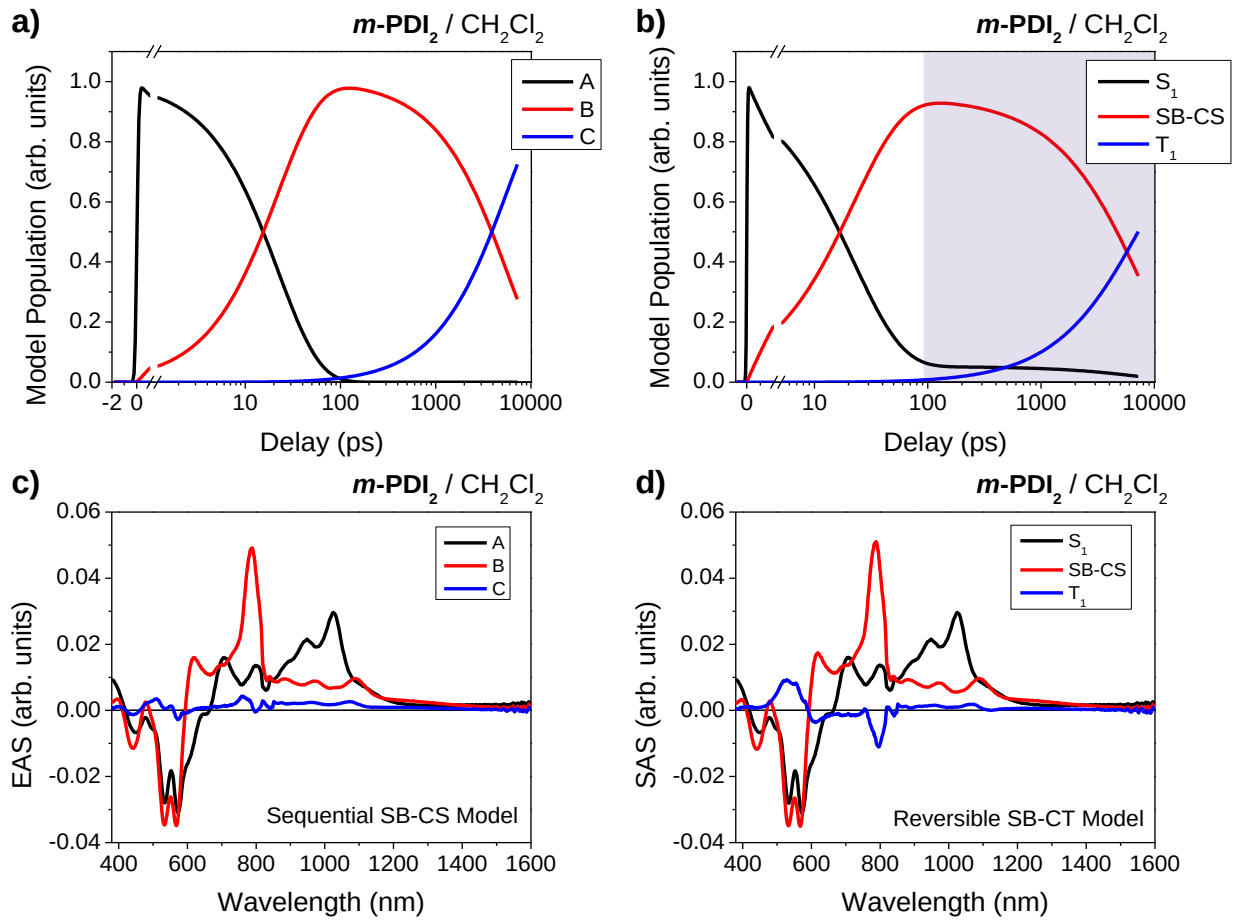


**Figure S46.** Comparison of the EAS- and SAS-computed populations (a,b) and spectra (c,d) for ***m*-PDI$_2$** in $CH_2Cl_2$ from fsTA data. The shaded area in the population plot highlights the reversible charge transfer.

Using these values, we can compute the populations of each species in the full kinetic model as a function of time and use them to deconvolute the spectra for each species in equilibrium. A comparison of the sequential evolution-associated spectra and the (equilibrium) species-associated spectra (SAS) is given for ***m*-PDI$_2$** below in $CH_2Cl_2$. Similar results are obtained for ***p*-PDI$_2$** in $CH_2Cl_2$. The primary differences in the spectra are for the final/triplet state; this is due to ambiguity in the rate constant for triplet generation, as it is not only difficult to determine with the ~8 ns window in the fsTA experiment, but separating charge recombination to the triplet state and to the singlet ground state cannot be done without a known triplet yield $\Phi_T$.

For ***m*-PDI$_2$** in toluene, the ratio of SB-CS state to $S_1$ (equilibrium constant) $K$ = 1.1, meaning the two states coexist in nearly one-to-one populations, so the spectral separation is imperfect. However, the increase in intensity near 600 nm and 800 nm in the second species as discussed in the text and loss of stimulated emission are consistent with the assignment of SB-CS.

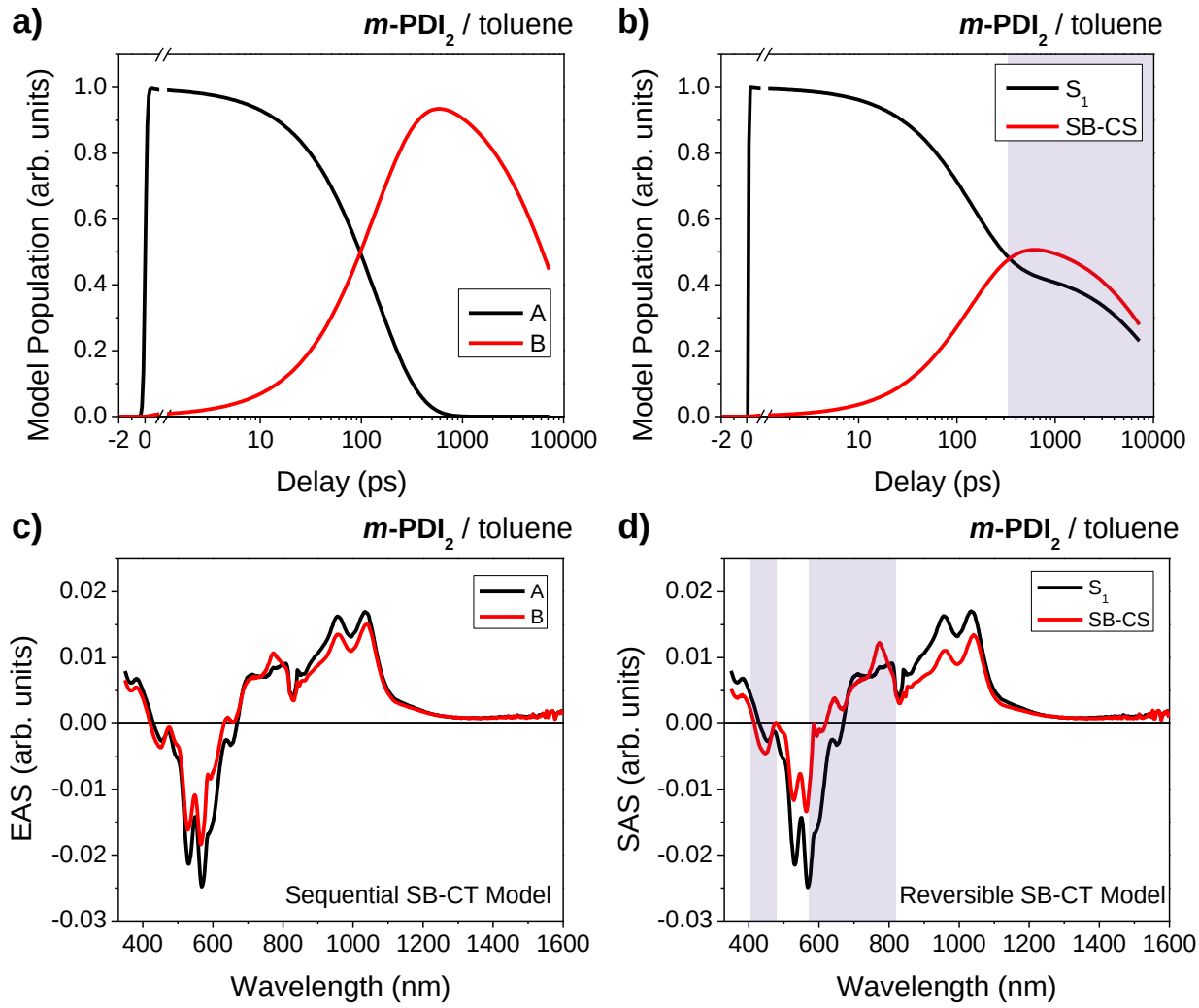


**Figure S47.** Comparison of the EAS- and SAS-computed populations (a,b) and spectra (c,d) for ***m*-PDI$_2$** in toluene. The shaded areas in the plots highlights the reversible charge transfer.

Similar results are obtained from the fsIR data of ***m*-PDI$_2$** in toluene-$d_8$, which exhibit similar rates in the evolution-associated spectra as shown above and give the same value for $K$. The species-associated spectra from the reversible charge transfer model do, however, show increased intensity between 1300-1330 cm$^{-1}$, deepening of the bleach at 1280 cm$^{-1}$, and the loss of intensity near 1450 cm$^{-1}$ all associated with

the SB-CS spectrum observed in $CD_2Cl_2$, as well as other more subtle changes. A comparison of the SAS in toluene-$d_8$ and $CD_2Cl_2$ is shown in Figure S48. Though the differences are subtle and the $S_1$ and SB-CS spectra cannot be fully isolated in toluene, the coexistence of each state is well-supported by the reversible charge-transfer model.

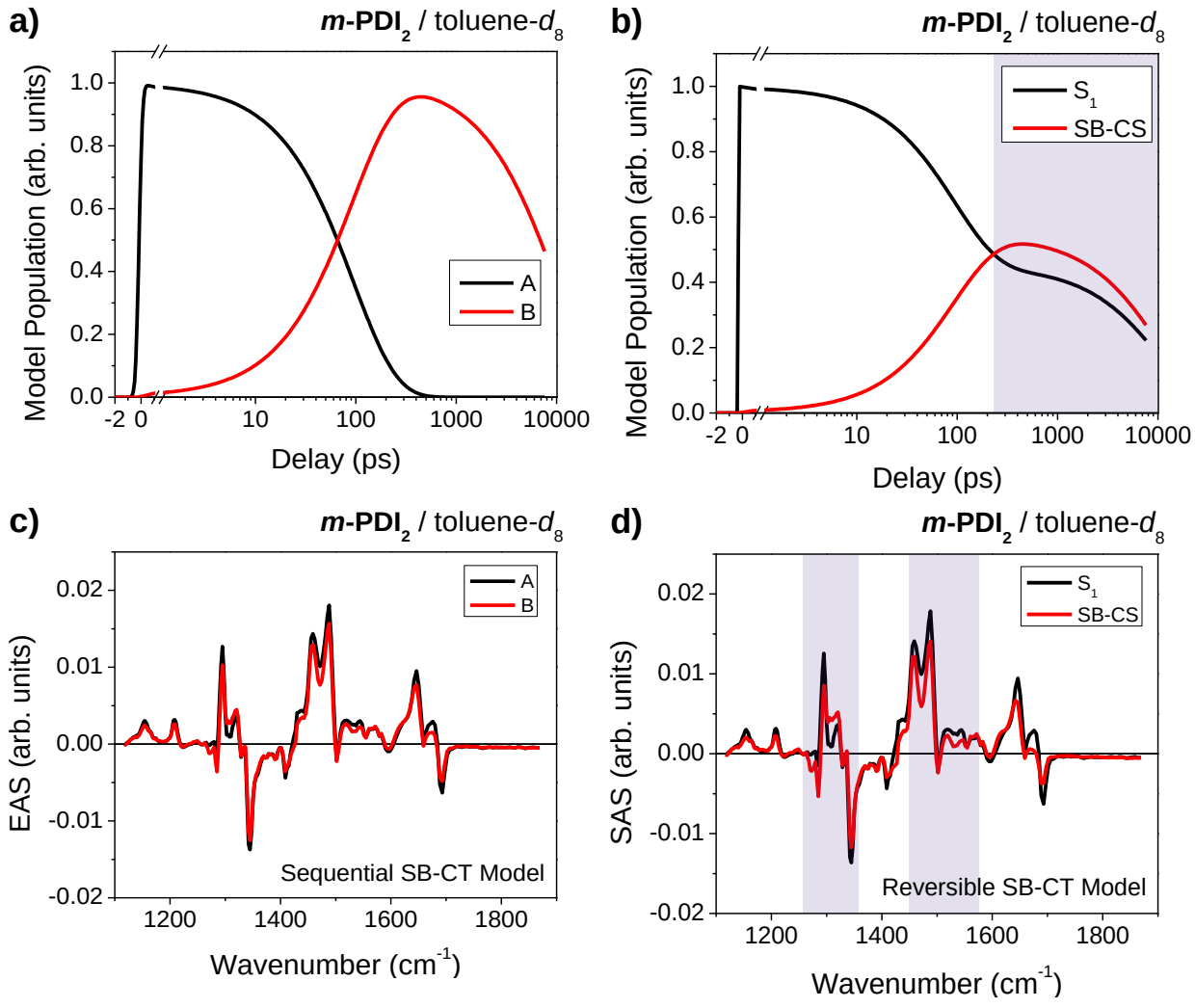


**Figure S48.** Comparison of the EAS- and SAS-computed populations (a,b) and spectra (c,d) for the fsIR data of ***m*-PDI$_2$** in toluene-$d_8$. The shaded areas in the plots highlight the reversible charge transfer.

Using eqs 2 and 3 in the main text we can examine the trends in the observed rates and correlated them to the differences in barriers for the different electron transfer processes by taking the ratio of rates assuming the electronic coupling only varies with distance $r_{DA}$:

$$\frac{k_{x2}}{k_{x1}} = e^{-\beta(r_2 - r_1)} \sqrt{\frac{\lambda_{tot,1}}{\lambda_{tot,2}}} e^{\frac{-\left(\Delta G_2^{\ddagger} - \Delta G_1^{\ddagger}\right)}{k_B T}} \quad \text{(S8)}$$

For the reverse electron transfer process, the driving force is opposite, leading to $\Delta G^{\ddagger} = (-\Delta G_{CS} + \lambda_{tot})^2/4\lambda_{tot}$. The ratios are evaluated for driving forces derived from both eq S9 below and the kinetic model. Disagreement in the toluene data are attributed to difference in electronic coupling as described in the text.

**Table S2.** Comparison of predicted ($k_{x2}$) and observed rate constants using eq S8 for the driving forces determined from eq S9 and from the kinetic model. For each entry $k_{x1}$ was set to the value for $k_1$ and $k_{-1}$ for ***m*-PDI$_2$** in $CH_2Cl_2$ from Table 3. The damping parameter was set to $\beta = 2.5$.

| Rate Constant | | ***m*-PDI$_2$ (toluene)** | ***p*-PDI$_2$ ($CH_2Cl_2$)** | **biph-PDI$_2$ ($CH_2Cl_2$)** |
|---|---|---|---|---|
| Exp. | $k_1$ | $(273\ \text{ps})^{-1}$ | $(23.5\ \text{ps})^{-1}$ | $(229\ \text{ps})^{-1}$ |
| | $k_{-1}$ | $(295\ \text{ps})^{-1}$ | $(443\ \text{ps})^{-1}$ | $(1088\ \text{ps})^{-1}$ |
| Weller | $k_1$ | $(166\ \text{ns})^{-1}$ | $(49\ \text{ps})^{-1}$ | $(148\ \text{ps})^{-1}$ |
| | $k_{-1}$ | $(4.2 \times 10^{-6}\ \text{ps})^{-1}$ | $(9.0\ \text{ns})^{-1}$ | $(95\ \text{ns})^{-1}$ |
| Model | $k_1$ | $(0.02\ \text{ps})^{-1}$ | $(243\ \text{ps})^{-1}$ | -- |
| | $k_{-1}$ | $(0.02\ \text{ps})^{-1}$ | $(1.1\ \text{ns})^{-1}$ | -- |

## 6. Driving Force ($\Delta G_{CS}$) Calculation

The driving force for SB-CS can be estimated using the equation developed by Weller:[4]

$$\Delta G_{CS} = e[E_{ox} - E_{red}] - \frac{e^2}{4\pi\varepsilon_0 \varepsilon r_{DA}} + \frac{e^2}{8\pi\varepsilon_0}\left(\frac{1}{r_+} + \frac{1}{r_-}\right)\left(\frac{1}{\varepsilon} - \frac{1}{\varepsilon'}\right) - E_{00} \quad \text{(S9)}$$

where $e$ is the charge of the electron, $E_{ox}$ and $E_{red}$ are the oxidation and reduction potentials, respectively, $\varepsilon_0$ is the permittivity of free space, $\varepsilon$ and $\varepsilon'$ are the static and optical dielectric constants of the solvent, respectively, $r_{DA}$ is the donor-acceptor distance, $r_+$ and $r_+$ are the cation and anion hard-sphere radii,

respectively, and $E_{00}$ is the energy of the excited singlet (donor) state. Because the donor-acceptor interaction here is between planes of the two tpPDIs, $r_+$ and $r_+$ are taken as a typical π-π stacking distance (3.5 Å),[5] similar to the C-atom van der Waals radius. Values for $r_{DA}$ were determined using force-field calculations (see below). These calculations suggest reasonably large driving forces for SB-CS in $CH_2Cl_2$, around -0.2 to -0.3 eV, which suggests large discrepancies between the optical and electrochemical bandgaps. Neglecting the Coulomb term in eq S9 yields significantly smaller driving forces (< 100 meV for ***m*-PDI$_2$** and ***p*-PDI$_2$**) for photo-induced SB-CS and implies much closer agreement between the optical and electrochemical bandgaps, as well as the kinetically determined $\Delta G_{CS}$.

**Table S3.** SB-CS energetic and structural parameters for ***m*-PDI$_2$**, ***p*-PDI$_2$**, and **biph-PDI$_2$** in $CH_2Cl_2$ and toluene. Driving forces and barriers are calculated using eq S9, $r_{DA}$ determined from MM+ calculations.

| | ***m*-PDI$_2$** | | ***p*-PDI$_2$** | | **biph-PDI$_2$** | |
|---|---|---|---|---|---|---|
| | Toluene | $CH_2Cl_2$ | Toluene | $CH_2Cl_2$ | Toluene | $CH_2Cl_2$ |
| $E_{ox}$ (V)* | -- | 1.3 | -- | 1.3 | -- | 1.29 |
| $E_{red}$ (V)* | -- | -0.81 | -- | -0.69 | -- | -0.69 |
| $E_{00}$ (eV) | 2.1 | 2.1 | 2.07 | 2.07 | 2.07 | 2.06 |
| $\Delta G_{IP}$ (eV) | 2.5 | 1.82 | 3.25 | 1.73 | 3.33 | 1.82 |
| $\Delta G_{CS}$ (eV) | 0.4 | -0.28 | 1.18 | -0.34 | 1.27 | -0.24 |
| $r_{DA}$ (Å) | 6.4 | 6.4 | 7.3 | 7.3 | 10.8 | 10.8 |
| $\Delta G^{\ddagger}$ (eV) | 0.4 | 0.17 | 1.18 | 0.18 | 1.29 | 0.28 |

As a comparison, we can also calculate the ion pair distance $r_{DA}$ that would be required to reproduce the measured driving forces using eq S9. For ***m*-PDI$_2$** in toluene, the necessary $r_{DA}$ is 4.7 Å, which is comparable to the π-stacking distance. However, in $CH_2Cl_2$, the effective distance reaches 21.9 Å in ***m*-PDI$_2$**, which is larger than the cyclophane itself. For ***p*-PDI$_2$** the agreement is even worse, with a negative distance of -44.8 Å. The unphysical values for these effective distances suggest that the Coulombic correction in eq S9 is overly simplistic and not fully accounting for the ionic interactions in these cyclophanes.

## 7. Computational Details

DFT calculations on a simplified surrogate structures of **PDI-Ref** monomer were performed using the Q-Chem 5.1 software package at the level of B3LYP/6-31G* *in vacuo*.[6] To lower the computational cost, methyl groups were substituted for the linkers and the tert-butyl groups of the phenoxy substituents. No imaginary frequencies were found in the final frequency output. Molecular structures of each dimer were calculated using the MMFF94 force field in Avogadro 1.2.0 for computing the average tpPDI distance.[7]

*Reorganization Energies.*

The total reorganization energy $\lambda_{tot}$ is taken as the sum of the solvent ($\lambda_S$) and internal ($\lambda_I$) reorganization energies: $\lambda_{tot} = \lambda_S + \lambda_I$. The solvent reorganization energy is computed using dielectric continuum theory:[8]

$$\lambda_S = \frac{e^2}{4\pi\varepsilon_0}\left(\frac{1}{2r_+} + \frac{1}{2r_-} - \frac{1}{r_{DA}}\right)\left(\frac{1}{n^2} - \frac{1}{\varepsilon}\right) \quad \text{(S10)}$$

where *n* is the solvent refractive index. The internal reorganization energy is calculated by taking the sum of the differences in the energy of the ionic states optimized at the $S_1$ electronic state geometry ($E_{(-)}^{ES}$ and $E_{(+)}^{ES}$) with the energy of the optimized ion geometries ($E_{(-)}^{opt}$ and $E_{(+)}^{opt}$):[9-10]

$$\lambda_I = E_{(-)}^{ES} - E_{(-)}^{opt} + E_{(+)}^{ES} - E_{(+)}^{opt} \quad \text{(S11)}$$

These values are obtained from DFT calculations of the tpPDI monomer reference (see below) and are given in Table S3. The relaxed/optimized excited state geometry was used since electron transfer is slow enough in all cases to follow vibrational relaxation from the vertically excited state.

**Table S4.** DFT-calculated energies and internal reorganization energy $\lambda_I$ for a tpPDI monomer.

| Energy | tpPDI |
|---|---|
| $E_{(+)}^{ES}$ (hartree) | -2791.81861 |
| $E_{(-)}^{ES}$ (hartree) | -2792.11726 |
| $E_{(+)}^{opt}$ (hartree) | -2791.82498 |
| $E_{(-)}^{opt}$ (hartree) | -2792.12247 |
| $\lambda_I$ (hartree) | 0.01158 |
| $\lambda_I$ (eV) | 0.315 |

*Calculated IR Spectra*

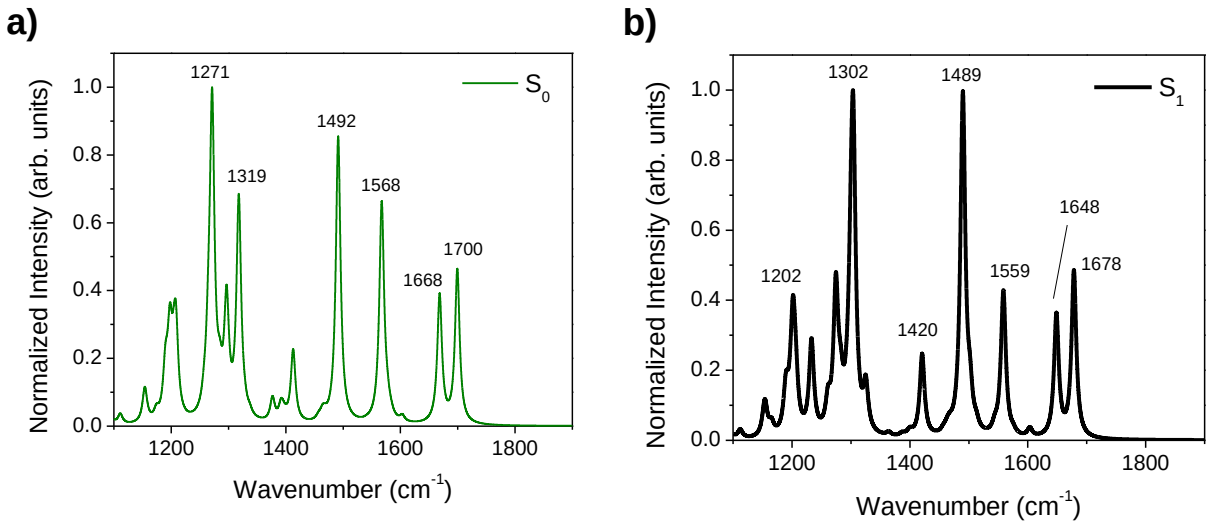


**Figure S49.** DFT-calculated IR spectra of the tpPDI singlet a) ground and b) excited states. The imide substituents were replaced with methyl groups for computational simplicity. Spectra were broadened using 10 $cm^{-1}$ Lorentzian lineshapes and normalized. The frequency axis was scaled by 0.96 to best match the experimental data.

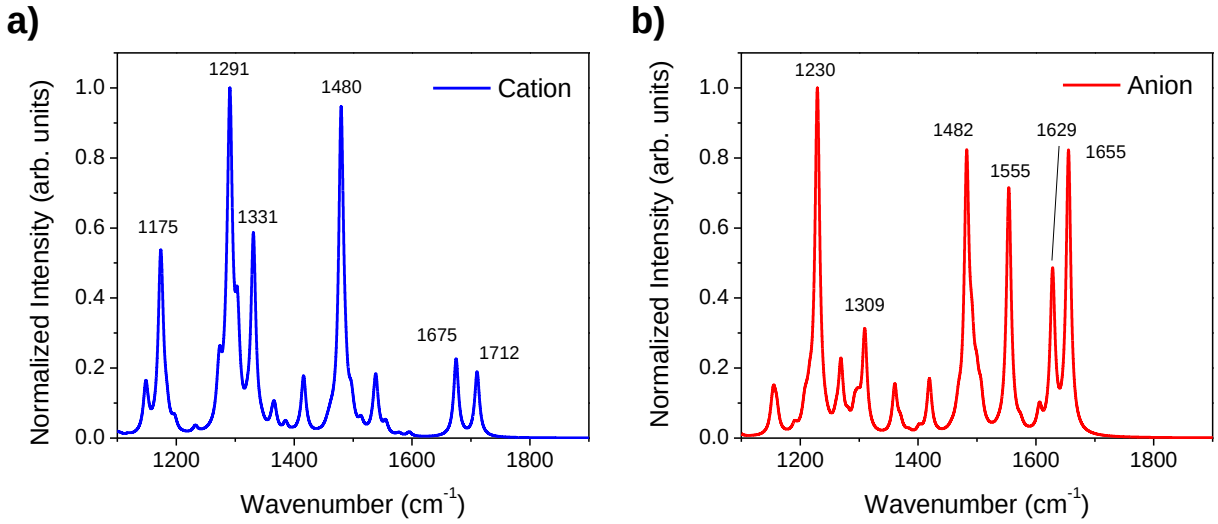


**Figure S50.** DFT-calculated IR spectra of the tpPDI a) cation and b) anion states. The imide substituents were replaced with methyl groups for computational simplicity. Spectra were broadened using 10 $cm^{-1}$ Lorentzian lineshapes and normalized. The frequency axis was scaled by 0.96 to best match the experimental data.

*Selected IR Mode Assignments*

**Table S5.** Selected IR Peak Assignments for the simplified tpPDI $S_0$.

| Exp. ($cm^{-1}$) | Calc ($cm^{-1}$) | Intensity (km/mol) | Assignment | Mode |
|---|---|---|---|---|
| 1278 | 1271.5 | 1543.7 | $\nu_{C=C}$<br>$\nu_{C-O}$ | 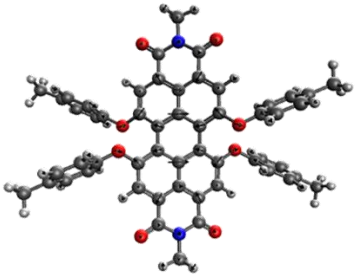 |
| 1339 | 1317.9 | 1113.9 | $\nu_{C=C}$<br>$\nu_{C-O}$ | 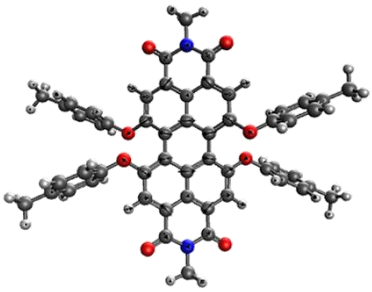 |
| 1500 | 1491.3 | 1217.4 | $\omega_{C-H}$ | 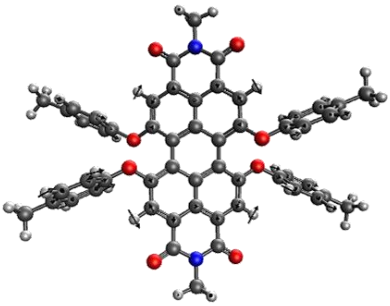 |
| 1584 | 1567.9 | 650.6 | $\nu_{C=C}$<br>$\omega_{C-H}$ | 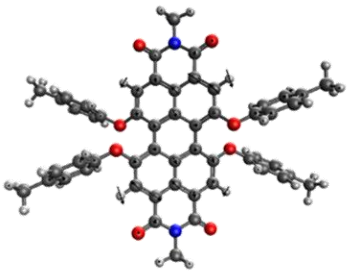 |
| 1692 | 1668.4<br>1699.3 | 577.2<br>778.6 | $\nu_{C=O}$<br>$\nu_{C=O}$ | 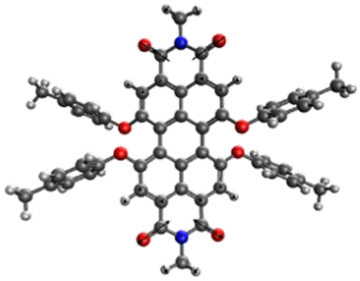 |

DFT / B3LYP; 6-31G*, scaling factor: 0.96. ν = stretch, ω = wag.

**Table S6.** Selected IR Peak Assignments for tpPDI $S_1$.

| Exp. ($cm^{-1}$) | Calc ($cm^{-1}$) | Intensity (km/mol) | Assignment | Mode |
|---|---|---|---|---|
| 1288 | 1303.9 | 1513.2 | $\nu_{C=C}$<br>$\nu_{C-O}$ | 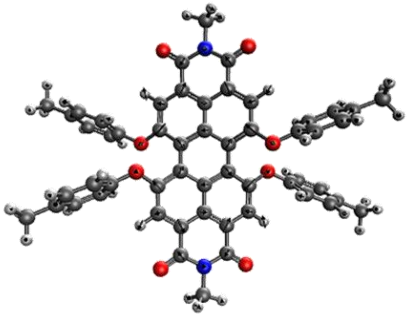 |
| 1487 | 1490.1 | 1576.5 | $\omega_{C-H}$ | 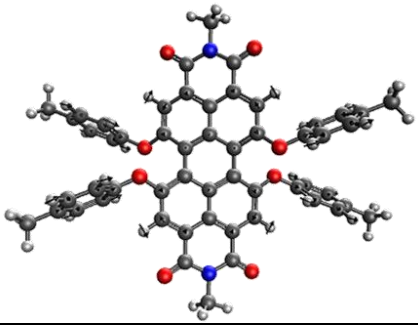 |
| 1558 | 1558.7 | 789.2 | $\nu_{C=C}$ | 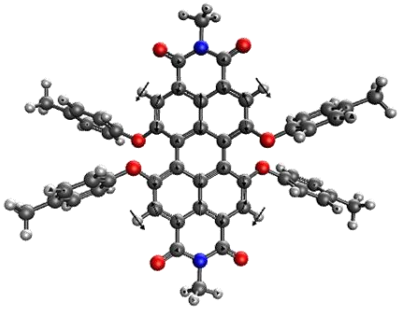 |
| 1651 | 1648.6<br>1678.3 | 579.9<br>923.6 | $\nu_{C=O}$<br>$\nu_{C=O}$ | 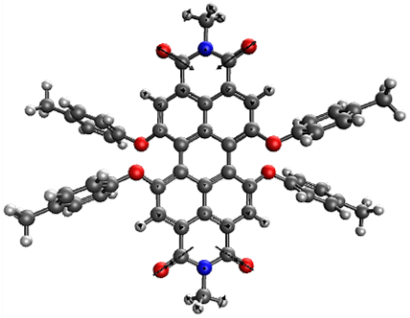 |

TD-DFT / B3LYP; 6-31G*, scaling factor: 0.96. ν = stretch, ω = wag.

**Table S7.** Selected IR Peak Assignments for the simplified tpPDI radical anion.

| Exp. ($cm^{-1}$) | Calc ($cm^{-1}$) | Intensity (km/mol) | Assignment | Mode |
|---|---|---|---|---|
| 1188 | 1229.1 | 2204.6 | $\nu_{C=C}$<br>$\nu_{C-O}$ | 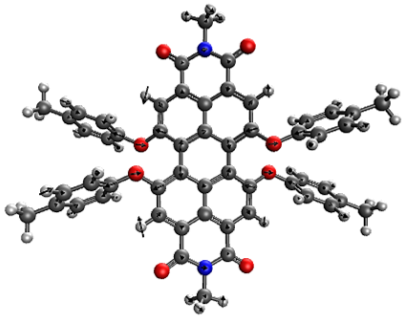 |
| 1480 | 1482.5 | 1721.7 | $\omega_{C-H}$ | 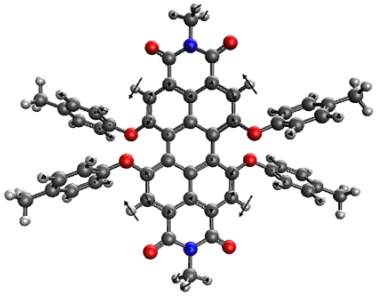 |
| 1560 | 1554.1 | 1579.3 | $\nu_{C=C}$<br>$\omega_{C-H}$ | 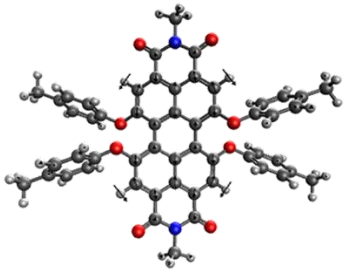 |
| 1630 | 1628.3<br>1655.4 | 872.3<br>1828.1 | $\nu_{C=O}$<br>$\nu_{C=O}$ | 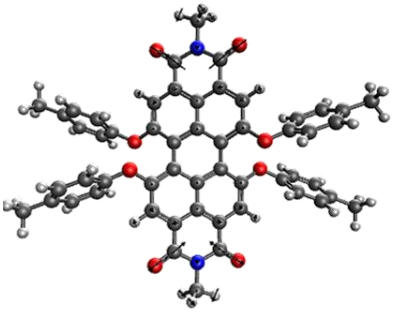 |

DFT / B3LYP; 6-31G*, scaling factor: 0.96. ν = stretch, ω = wag.

**Table S8.** Selected IR Peak Assignments for the simplified tpPDI radical cation.

| Exp. ($cm^{-1}$) | Calc ($cm^{-1}$) | Intensity (km/mol) | Assignment | Mode |
|---|---|---|---|---|
| 1302 | 1291.1 | 1792.9 | $\nu_{C=C}$ $\nu_{C-O}$ | 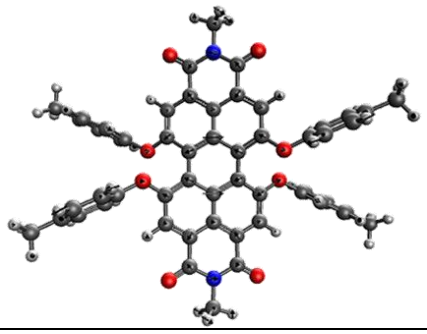 |
| 1320 | 1330.9 | 1215.0 | $\nu_{C=C}$ $\nu_{C-O}$ | 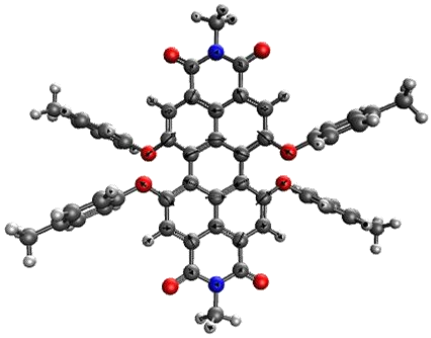 |
| 1480 | 1479.5 | 1962.0 | $\omega_{C-H}$ | 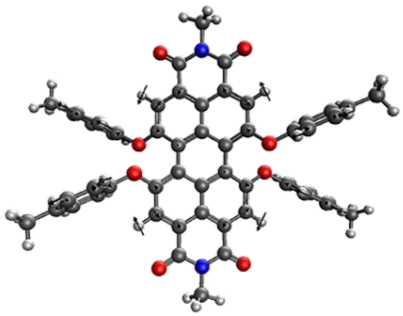 |
| 1515 | 1538.6 | 340.3 | $\nu_{C=C}$ | 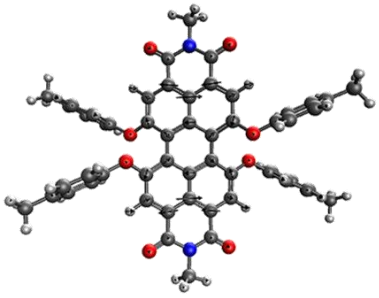 |

DFT / B3LYP; 6-31G*, scaling factor: 0.96. ν = stretch, ω = wag.

*Geometry Tables*

*i. DFT-calculated structures*

**Table S9**. Geometry tables for tpPDI $S_0$ and $S_1$ structures.

| **tpPDI** $S_0$ | | | | **tpPDI** $S_1$ | | | |
|---|---|---|---|---|---|---|---|
| QChem 5.1, B3LYP/6-31G* | | | | QChem 5.1, TD-DFT B3LYP/6-31G* | | | |
| $E_h$ = -2792.04903274 | | | | $E_h$ = -2792.0452818403 | | | |
| **Atom** | **X** | **Y** | **Z** | **Atom** | **X** | **Y** | **Z** |
| O | 2.18396 | -5.66435 | -0.64492 | O | -3.42507 | -0.75663 | 1.08643 |
| O | -2.22357 | -5.65544 | 0.59937 | O | -3.43202 | 0.73750 | -1.06519 |
| O | 2.23032 | 5.66078 | 0.57033 | O | 3.42933 | -0.73123 | -1.07196 |
| O | -2.18212 | 5.66690 | -0.65642 | O | 3.42439 | 0.75883 | 1.08265 |
| O | -3.41017 | 0.75084 | -1.12392 | O | 2.16731 | 5.67719 | 0.71023 |
| O | -3.41361 | -0.71465 | 1.10442 | O | -2.19516 | 5.67775 | -0.65871 |
| O | 3.41791 | 0.71995 | 1.09309 | O | 2.19030 | -5.67130 | -0.68115 |
| O | 3.41022 | -0.74951 | -1.13063 | O | -2.16830 | -5.67381 | 0.70004 |
| N | -0.02731 | -5.65670 | -0.02109 | N | -0.02107 | 5.67666 | 0.02313 |
| N | 0.03183 | 5.66059 | -0.04210 | N | 0.01808 | -5.67175 | 0.00660 |
| C | 2.33205 | -2.85535 | -0.67270 | C | -8.61034 | -3.06186 | 1.67967 |
| C | 2.36444 | -1.46508 | -0.62032 | C | 8.61182 | -3.03127 | -1.71020 |
| C | 1.23534 | -0.71040 | -0.16126 | C | -8.62609 | 2.99941 | -1.74021 |
| C | -0.00560 | -1.40920 | -0.01533 | C | 8.63150 | 3.02003 | 1.65321 |
| C | -0.01261 | -2.83537 | -0.01570 | C | 5.27551 | -1.31857 | -2.45891 |
| C | 1.16951 | -3.54342 | -0.32505 | C | 6.55590 | -1.85182 | -2.61119 |
| C | -1.23976 | -0.69818 | 0.13074 | C | -6.56415 | -1.87799 | 2.59779 |
| C | -2.37607 | -1.44089 | 0.59250 | C | -5.28288 | -1.34339 | 2.45627 |
| C | -2.35784 | -2.83152 | 0.64284 | C | -4.66767 | -1.37167 | 1.20816 |
| C | -1.20249 | -3.52975 | 0.29275 | C | -5.31956 | -1.92206 | 0.10390 |
| C | -1.22185 | -5.00385 | 0.31420 | C | -6.59420 | -2.45925 | 0.26723 |
| C | 1.17994 | -5.01919 | -0.35381 | C | -7.23873 | -2.45016 | 1.51291 |
| C | 1.24282 | 0.70260 | 0.12467 | C | 6.61075 | -2.42287 | -0.27848 |
| C | 0.00839 | 1.41320 | -0.01995 | C | 5.33654 | -1.88737 | -0.10465 |
| C | -1.23302 | 0.71399 | -0.15987 | C | 4.67280 | -1.34297 | -1.20441 |
| C | 2.38075 | 1.44629 | 0.58098 | C | 7.24226 | -2.41861 | -1.53055 |
| C | 2.36362 | 2.83712 | 0.62552 | C | -5.35041 | 1.88274 | -0.10893 |
| C | 1.20720 | 3.53428 | 0.27633 | C | -6.62265 | 2.42316 | -0.29367 |
| C | 0.01587 | 2.83937 | -0.02531 | C | -7.23899 | 2.43009 | -1.55143 |
| C | -1.16712 | 3.54674 | -0.33314 | C | -6.53682 | 1.87894 | -2.63202 |
| C | -2.33093 | 2.85770 | -0.67468 | C | -5.26105 | 1.34156 | -2.46894 |
| C | -2.36321 | 1.46762 | -0.61802 | C | -4.67481 | 1.34919 | -1.20497 |
| C | 1.22732 | 5.00854 | 0.29128 | C | 5.28803 | 1.33838 | 2.44677 |
| C | -1.17708 | 5.02238 | -0.36746 | C | 6.57343 | 1.86566 | 2.58372 |
| C | 0.07394 | 7.12551 | -0.04626 | C | 7.24779 | 2.43295 | 1.49699 |
| C | -0.06858 | -7.12164 | -0.01891 | C | 6.59694 | 2.45008 | 0.25391 |
| C | -4.66498 | 1.33338 | -1.26557 | C | 5.31896 | 1.92101 | 0.09527 |
| C | -5.33280 | 1.90480 | -0.17999 | C | 4.66885 | 1.37069 | 1.20134 |
| C | -6.62105 | 2.39835 | -0.36186 | C | 0.05596 | -7.13739 | -0.00131 |
| C | -7.26385 | 2.32988 | -1.60791 | C | -0.05956 | 7.14231 | 0.02039 |
| C | -6.57104 | 1.74351 | -2.67328 | C | 1.17559 | 5.03580 | 0.38748 |
| C | -5.27659 | 1.24696 | -2.51288 | C | -1.20749 | 5.02554 | -0.34458 |
| C | 4.66769 | 1.30386 | 1.27565 | C | 2.34366 | 1.45906 | 0.62258 |
| C | 5.22455 | 1.24692 | 2.55211 | C | 2.30593 | 2.86246 | 0.70733 |
| C | 6.50514 | 1.75550 | 2.75987 | C | 1.16352 | 3.55358 | 0.35485 |
| C | 7.24278 | 2.32406 | 1.71180 | C | -0.01089 | 2.84762 | 0.01312 |

| | | | | | | | |
|---|---|---|---|---|---|---|---|
| C | 6.65639 | 2.36320 | 0.43995 | C | -1.19107 | 3.54487 | -0.32470 |
| C | 5.37863 | 1.85524 | 0.21050 | C | -2.32895 | 2.84870 | -0.68083 |
| C | -7.24902 | -2.30910 | 1.68123 | C | -2.35634 | 1.44452 | -0.60380 |
| C | -4.66533 | -1.29769 | 1.27559 | C | 1.23516 | 0.72340 | 0.15609 |
| C | -5.36439 | -1.85207 | 0.20216 | C | -0.00594 | 1.42429 | 0.00977 |
| C | -6.64577 | -2.35314 | 0.41547 | C | -1.24222 | 0.71552 | -0.13971 |
| C | 7.25437 | -2.34726 | -1.63064 | C | -1.17731 | -5.03166 | 0.37654 |
| C | 6.61967 | -2.40597 | -0.38069 | C | 1.20371 | -5.01981 | -0.36211 |
| C | 5.33479 | -1.90434 | -0.19273 | C | 1.18781 | -3.53924 | -0.33718 |
| C | 4.66335 | -1.33474 | -1.27630 | C | 2.32494 | -2.84210 | -0.69352 |
| C | 5.26916 | -1.25397 | -2.52742 | C | 2.35318 | -1.43823 | -0.61129 |
| C | 6.55945 | -1.75778 | -2.69379 | C | 1.23998 | -0.71020 | -0.14366 |
| C | -6.52692 | -1.73386 | 2.73421 | C | -1.16506 | -3.54940 | 0.34789 |
| C | -5.23994 | -1.23081 | 2.54213 | C | 0.00863 | -2.84264 | 0.00549 |
| C | -8.65756 | 2.88427 | -1.78831 | C | 0.00378 | -1.41932 | 0.00599 |
| C | 8.63377 | 2.86369 | 1.94964 | C | -1.23702 | -0.71878 | 0.15635 |
| C | -8.62647 | -2.88852 | 1.90237 | C | -2.34470 | -1.45551 | 0.62318 |
| C | 8.63653 | -2.92540 | -1.82386 | C | -2.30666 | -2.85911 | 0.70450 |
| H | 3.18813 | -3.42538 | -1.01057 | H | 8.54308 | -4.11044 | -1.90153 |
| H | -3.21918 | -3.39423 | 0.97973 | H | 9.14347 | -2.58387 | -2.55651 |
| H | 3.22633 | 3.40094 | 0.95699 | H | 9.22951 | -2.90031 | -0.81507 |
| H | -3.18803 | 3.42658 | -1.01202 | H | 9.30552 | 2.67350 | 0.86105 |
| H | 0.83189 | 7.47151 | -0.75354 | H | 8.61013 | 4.11634 | 1.60128 |
| H | -0.91201 | 7.48376 | -0.33387 | H | 9.07443 | 2.74448 | 2.61536 |
| H | -0.82815 | -7.47121 | -0.72272 | H | -9.23822 | -2.88373 | 0.79962 |
| H | 0.91683 | -7.48053 | -0.30756 | H | -8.54754 | -4.14952 | 1.81729 |
| H | -7.14176 | 2.83748 | 0.48593 | H | -9.12830 | -2.65172 | 2.55272 |
| H | -7.04635 | 1.67566 | -3.64868 | H | -8.67530 | 3.65267 | -2.61903 |
| H | -4.73843 | 0.79448 | -3.33993 | H | -9.36880 | 2.20441 | -1.88758 |
| H | 6.93494 | 1.71598 | 3.75818 | H | -8.93955 | 3.58432 | -0.86985 |
| H | 7.20913 | 2.79468 | -0.39089 | H | -0.30420 | 7.50412 | -0.98133 |
| H | 4.93850 | 1.87787 | -0.78081 | H | 0.29843 | -7.49577 | -1.00480 |
| H | -4.91264 | -1.87428 | -0.78390 | H | 4.74163 | -0.88240 | -3.29754 |
| H | -7.19098 | -2.78042 | -0.42281 | H | 7.02504 | -1.83043 | -3.59196 |
| H | 7.14310 | -2.84506 | 0.46535 | H | 4.83034 | 1.91907 | -0.87355 |
| H | 4.85892 | -1.93749 | 0.78158 | H | -4.71326 | 0.92097 | -3.30655 |
| H | 4.72883 | -0.80026 | -3.35240 | H | -7.04311 | -1.85335 | 3.57367 |
| H | 7.02986 | -1.69471 | -3.67200 | H | -4.75809 | -0.90320 | 3.29852 |
| H | 4.64957 | 0.81339 | 3.36444 | H | -4.83539 | -1.91501 | -0.86713 |
| H | -4.85104 | 1.94438 | 0.79117 | H | -7.10144 | -2.88614 | -0.59487 |
| H | -6.97315 | -1.68138 | 3.72438 | H | 7.12748 | -2.84496 | 0.58030 |
| H | -4.67858 | -0.78805 | 3.35898 | H | 4.86200 | -1.87737 | 0.87107 |
| H | -0.33439 | -7.48370 | 0.97756 | H | -4.88569 | 1.86831 | 0.87144 |
| H | 0.34256 | 7.49174 | 0.94793 | H | -7.14730 | 2.84295 | 0.56112 |
| H | 8.98443 | 3.45335 | 1.09694 | H | -6.99054 | 1.87610 | -3.62053 |
| H | 9.35645 | 2.05279 | 2.10960 | H | 4.76396 | 0.90089 | 3.29085 |
| H | 8.66796 | 3.50478 | 2.83814 | H | 7.05596 | 1.83760 | 3.55766 |
| H | 9.13976 | -2.48233 | -2.68941 | H | 7.10272 | 2.87547 | -0.60990 |
| H | 8.59397 | -4.01007 | -1.98988 | H | -0.92326 | -7.49550 | 0.30823 |
| H | 9.26704 | -2.75848 | -0.94356 | H | 0.82969 | -7.49111 | 0.68461 |
| H | -9.09302 | 2.56807 | -2.74136 | H | 0.92014 | 7.49974 | 0.32919 |
| H | -8.65611 | 3.98196 | -1.77405 | H | -0.83205 | 7.49324 | 0.70912 |
| H | -9.32692 | 2.55339 | -0.98564 | H | 3.17218 | 3.42084 | 1.03951 |
| H | -9.26370 | -2.75245 | 1.02186 | H | -3.19917 | 3.40372 | -1.00833 |
| H | -9.12635 | -2.42203 | 2.75767 | H | 3.19427 | -3.39613 | -1.02509 |
| H | -8.57609 | -3.96717 | 2.10220 | H | -3.17217 | -3.41846 | 1.03693 |

**Table S10**. Geometry tables for $tpPDI^{-\bullet}$ and $tpPDI^{+\bullet}$ structures.

| **$tpPDI^{-\bullet}$** | | | | **$tpPDI^{+\bullet}$** | | | |
|---|---|---|---|---|---|---|---|
| QChem 5.1, B3LYP/6-31G* | | | | QChem 5.1, B3LYP/6-31G* | | | |
| $E_h$ = -2792.1224705237 | | | | $E_h$ = -2791.8249820416 | | | |
| **Atom** | **X** | **Y** | **Z** | **Atom** | **X** | **Y** | **Z** |
| O | 2.19993 | -5.66912 | -0.67124 | O | 2.23172 | -5.64876 | -0.54600 |
| O | -2.18280 | -5.68444 | 0.66520 | O | -2.19415 | -5.66119 | 0.60445 |
| O | 2.17530 | 5.69262 | 0.68531 | O | 2.20849 | 5.66844 | 0.54290 |
| O | -2.19782 | 5.67545 | -0.68193 | O | -2.22178 | 5.64917 | -0.59043 |
| O | -3.42886 | 0.74177 | -1.11861 | O | -3.41927 | 0.75355 | -1.04782 |
| O | -3.43612 | -0.73602 | 1.10935 | O | -3.41517 | -0.75547 | 1.06735 |
| O | 3.43341 | 0.74702 | 1.12722 | O | 3.42386 | 0.76391 | 1.05172 |
| O | 3.43839 | -0.73563 | -1.09302 | O | 3.42232 | -0.75595 | -1.05485 |
| N | 0.00033 | -5.65212 | -0.00072 | N | 0.01157 | -5.67808 | 0.02872 |
| N | -0.00310 | 5.65942 | 0.00428 | N | 0.00073 | 5.68186 | -0.02507 |
| C | 2.32971 | -2.83641 | -0.68837 | C | 2.35527 | -2.85959 | -0.59389 |
| C | 2.36189 | -1.45337 | -0.59362 | C | 2.38023 | -1.45703 | -0.57545 |
| C | 1.24081 | -0.70612 | -0.13390 | C | 1.24363 | -0.70575 | -0.13025 |
| C | 0.00088 | -1.41377 | 0.00675 | C | 0.00544 | -1.40820 | 0.01068 |
| C | 0.00059 | -2.84576 | 0.00521 | C | 0.00729 | -2.83126 | 0.01656 |
| C | 1.18207 | -3.54751 | -0.32693 | C | 1.19420 | -3.53685 | -0.26803 |
| C | -1.23953 | -0.70688 | 0.14845 | C | -1.23477 | -0.70738 | 0.14552 |
| C | -2.36105 | -1.45384 | 0.60724 | C | -2.37041 | -1.45758 | 0.59481 |
| C | -2.32928 | -2.83721 | 0.69945 | C | -2.34130 | -2.85991 | 0.62797 |
| C | -1.18155 | -3.54607 | 0.33576 | C | -1.17812 | -3.53583 | 0.30865 |
| C | -1.19699 | -5.00764 | 0.35778 | C | -1.18666 | -5.02779 | 0.33488 |
| C | 1.20437 | -5.00992 | -0.35694 | C | 1.21364 | -5.03105 | -0.28116 |
| C | 1.23979 | 0.71408 | 0.15591 | C | 1.24260 | 0.71217 | 0.13547 |
| C | -0.00024 | 1.42092 | 0.00732 | C | 0.00237 | 1.41210 | -0.00085 |
| C | -1.23906 | 0.71307 | -0.14104 | C | -1.23664 | 0.70877 | -0.13152 |
| C | 2.35820 | 1.46197 | 0.62028 | C | 2.37987 | 1.46491 | 0.57679 |
| C | 2.32420 | 2.84530 | 0.71447 | C | 2.35255 | 2.86741 | 0.59682 |
| C | 1.17832 | 3.55386 | 0.34540 | C | 1.18887 | 3.54123 | 0.27426 |
| C | -0.00109 | 2.85285 | 0.00649 | C | 0.00171 | 2.83516 | -0.00710 |
| C | -1.18072 | 3.55425 | -0.33316 | C | -1.18544 | 3.53908 | -0.29453 |
| C | -2.32534 | 2.84260 | -0.70292 | C | -2.34818 | 2.85971 | -0.60972 |
| C | -2.35747 | 1.45960 | -0.60816 | C | -2.37450 | 1.45733 | -0.57788 |
| C | 1.19234 | 5.01549 | 0.36983 | C | 1.19924 | 5.03340 | 0.28410 |
| C | -1.20350 | 5.01663 | -0.36307 | C | -1.20326 | 5.03309 | -0.32343 |
| C | 0.02768 | 7.11968 | 0.01179 | C | 0.03426 | 7.15288 | -0.03023 |
| C | -0.03223 | -7.11235 | 0.00294 | C | -0.01979 | -7.14911 | 0.04054 |
| C | -4.68838 | 1.29695 | -1.16321 | C | -4.65084 | 1.38306 | -1.31083 |
| C | -5.27917 | 1.92312 | -0.06032 | C | -5.43729 | 1.85447 | -0.26180 |
| C | -6.58611 | 2.39050 | -0.15704 | C | -6.68398 | 2.40257 | -0.55458 |
| C | -7.33422 | 2.24524 | -1.33500 | C | -7.15784 | 2.47968 | -1.87334 |
| C | -6.72417 | 1.60901 | -2.42074 | C | -6.34301 | 1.98226 | -2.89850 |
| C | -5.41170 | 1.14116 | -2.34528 | C | -5.08843 | 1.43256 | -2.62859 |
| C | 4.69366 | 1.30191 | 1.15540 | C | 4.65140 | 1.39520 | 1.32754 |
| C | 5.42906 | 1.15187 | 2.33261 | C | 5.07476 | 1.44108 | 2.65171 |
| C | 6.73809 | 1.62662 | 2.39662 | C | 6.32041 | 1.99820 | 2.93808 |
| C | 7.33658 | 2.26242 | 1.30201 | C | 7.14511 | 2.50534 | 1.92292 |
| C | 6.57618 | 2.40651 | 0.13402 | C | 6.68419 | 2.43684 | 0.60096 |
| C | 5.26996 | 1.93046 | 0.04826 | C | 5.44397 | 1.87904 | 0.29095 |
| C | -7.33604 | -2.25349 | 1.32647 | C | -7.16220 | -2.48182 | 1.85287 |

| | | | | | | | |
|---|---|---|---|---|---|---|---|
| C | -4.69380 | -1.29573 | 1.15482 | C | -4.65004 | -1.38308 | 1.31615 |
| C | -5.28305 | -1.92181 | 0.05111 | C | -5.41285 | -1.88151 | 0.26289 |
| C | -6.58823 | -2.39409 | 0.14774 | C | -6.66263 | -2.43075 | 0.54317 |
| C | 7.32987 | -2.27197 | -1.32762 | C | 7.13700 | -2.50575 | -1.93744 |
| C | 6.58673 | -2.40800 | -0.14532 | C | 6.69616 | -2.39949 | -0.60931 |
| C | 5.28441 | -1.92904 | -0.04345 | C | 5.45789 | -1.84252 | -0.29752 |
| C | 4.69339 | -1.30120 | -1.14524 | C | 4.64687 | -1.39168 | -1.33664 |
| C | 5.41136 | -1.15496 | -2.33148 | C | 5.05144 | -1.46999 | -2.66352 |
| C | 6.71965 | -1.63389 | -2.41212 | C | 6.29799 | -2.02820 | -2.95258 |
| C | -6.72755 | -1.61715 | 2.41303 | C | -6.37166 | -1.95374 | 2.88295 |
| C | -5.41673 | -1.14458 | 2.33762 | C | -5.11527 | -1.40391 | 2.62604 |
| C | -8.74792 | 2.77269 | -1.42631 | C | -8.50244 | 3.09775 | -2.17355 |
| C | 8.76426 | 2.75480 | 1.36995 | C | 8.49974 | 3.08786 | 2.24799 |
| C | -8.74817 | -2.78520 | 1.41759 | C | -8.50404 | -3.10940 | 2.14514 |
| C | 8.73914 | -2.81033 | -1.42478 | C | 8.47189 | -3.13457 | -2.25802 |
| H | 3.18685 | -3.39311 | -1.04685 | H | 3.23080 | -3.42657 | -0.88338 |
| H | -3.18625 | -3.39523 | 1.05660 | H | -3.21424 | -3.42764 | 0.92404 |
| H | 3.17913 | 3.40327 | 1.07661 | H | 3.22721 | 3.43698 | 0.88420 |
| H | -3.18025 | 3.39849 | -1.06803 | H | -3.22395 | 3.42483 | -0.90212 |
| H | 0.79680 | 7.48170 | -0.67684 | H | 0.78439 | 7.49782 | -0.74481 |
| H | -0.95690 | 7.46945 | -0.29239 | H | -0.95456 | 7.50752 | -0.31088 |
| H | -0.80244 | -7.47111 | -0.68606 | H | -0.77363 | -7.50323 | -0.66556 |
| H | 0.95182 | -7.46251 | -0.30253 | H | 0.96792 | -7.50552 | -0.24176 |
| H | -7.03862 | 2.87093 | 0.70832 | H | -7.30403 | 2.76873 | 0.25955 |
| H | -7.28034 | 1.48083 | -3.34734 | H | -6.69078 | 2.02526 | -3.92714 |
| H | -4.93703 | 0.65103 | -3.18990 | H | -4.45828 | 1.04697 | -3.42380 |
| H | 7.30051 | 1.50841 | 3.32110 | H | 6.65382 | 2.04307 | 3.97167 |
| H | 7.01609 | 2.89650 | -0.73210 | H | 7.30623 | 2.81926 | -0.20377 |
| H | 4.69479 | 2.04245 | -0.86425 | H | 5.10111 | 1.81316 | -0.73666 |
| H | -4.71898 | -2.02579 | -0.86930 | H | -5.04183 | -1.82629 | -0.75553 |
| H | -7.03954 | -2.87463 | -0.71818 | H | -7.26369 | -2.81877 | -0.27490 |
| H | 7.03954 | -2.89017 | 0.71892 | H | 7.33536 | -2.75014 | 0.19679 |
| H | 4.72351 | -2.02920 | 0.87935 | H | 5.13057 | -1.74486 | 0.73254 |
| H | 4.93649 | -0.66345 | -3.17516 | H | 4.40276 | -1.09938 | -3.45090 |
| H | 7.27219 | -1.51315 | -3.34184 | H | 6.62008 | -2.09399 | -3.98833 |
| H | 4.96095 | 0.66783 | 3.18441 | H | 4.43550 | 1.05248 | 3.43814 |
| H | -4.71502 | 2.03082 | 0.85960 | H | -5.08544 | 1.77854 | 0.76203 |
| H | -7.28363 | -1.49264 | 3.34017 | H | -6.74057 | -1.97371 | 3.90510 |
| H | -4.94322 | -0.65433 | 3.18281 | H | -4.50331 | -0.99648 | 3.42458 |
| H | -0.28128 | -7.47936 | 1.00299 | H | -0.28387 | -7.50260 | 1.03971 |
| H | 0.27718 | 7.48380 | 1.01268 | H | 0.30478 | 7.51730 | 0.96325 |
| H | 8.94392 | 3.56051 | 0.64966 | H | 8.87921 | 3.70314 | 1.42683 |
| H | 9.48101 | 1.95249 | 1.14492 | H | 9.23575 | 2.29501 | 2.43344 |
| H | 9.01105 | 3.13648 | 2.36763 | H | 8.46135 | 3.71004 | 3.14840 |
| H | 9.23330 | -2.46580 | -2.33951 | H | 8.80904 | -2.86991 | -3.26472 |
| H | 8.75425 | -3.90861 | -1.43651 | H | 8.41306 | -4.22930 | -2.20705 |
| H | 9.35285 | -2.49095 | -0.57324 | H | 9.24396 | -2.81910 | -1.54801 |
| H | -9.24775 | 2.41433 | -2.33269 | H | -8.85998 | 2.81703 | -3.16879 |
| H | -8.77070 | 3.87068 | -1.45078 | H | -8.44831 | 4.19337 | -2.13927 |
| H | -9.35197 | 2.45910 | -0.56581 | H | -9.25722 | 2.78873 | -1.44237 |
| H | -9.35630 | -2.46393 | 0.56277 | H | -9.19023 | -2.99916 | 1.29959 |
| H | -9.24519 | -2.43745 | 2.32959 | H | -8.97430 | -2.66113 | 3.02601 |
| H | -8.76829 | -3.88340 | 1.43052 | H | -8.39921 | -4.18408 | 2.34269 |

## 8. References for Supporting Information


1. Schultz, J. D.; Coleman, A. F.; Mandal, A.; Shin, J. Y.; Ratner, M. A.; Young, R. M.; Wasielewski, M. R., Steric interactions impact vibronic and vibrational coherences in perylenediimide cyclophanes. *J. Phys. Chem. Lett.* **2019,** *10*, 7498-7504.

2. von Krbek, L. K. S.; Achazi, A. J.; Schoder, S.; Gaedke, M.; Biberger, T.; Paulus, B.; Schalley, C. A., The delicate balance of preorganisation and adaptability in multiply bonded host–guest complexes. *Chem. Eur. J.* **2017,** *23*, 2877-2883.

3. Spenst, P.; Young, R. M.; Wasielewski, M. R.; Würthner, F., Guest and solvent modulated photo-driven charge separation and triplet generation in a perylene bisimide cyclophane. *Chem. Sci.* **2016,** *7*, 5428-5434.

4. Weller, A., Photoinduced electron transfer in solution: Exciplex and radical ion pair formation free enthalpies and their solvent dependence. *Z. Phys. Chem* . **1982,** *133*, 93-98.

5. Würthner, F., Perylene bisimide dyes as versatile building blocks for functional supramolecular architectures. *Chem. Commun.* **2004**, 1564-1579.

6. Shao, Y.; Gan, Z.; Epifanovsky, E.; Gilbert, A. T. B.; Wormit, M.; Kussmann, J.; Lange, A. W.; Behn, A.; Deng, J.; Feng, X.; Ghosh, D.; Goldey, M.; Horn, P. R.; Jacobson, L. D.; Kaliman, I.; Khaliullin, R. Z.; Kuś, T.; Landau, A.; Liu, J.; Proynov, E. I.; Rhee, Y. M.; Richard, R. M.; Rohrdanz, M. A.; Steele, R. P.; Sundstrom, E. J.; Woodcock, H. L.; Zimmerman, P. M.; Zuev, D.; Albrecht, B.; Alguire, E.; Austin, B.; Beran, G. J. O.; Bernard, Y. A.; Berquist, E.; Brandhorst, K.; Bravaya, K. B.; Brown, S. T.; Casanova, D.; Chang, C.-M.; Chen, Y.; Chien, S. H.; Closser, K. D.; Crittenden, D. L.; Diedenhofen, M.; DiStasio, R. A.; Do, H.; Dutoi, A. D.; Edgar, R. G.; Fatehi, S.; Fusti-Molnar, L.; Ghysels, A.; Golubeva-Zadorozhnaya, A.; Gomes, J.; Hanson-Heine, M. W. D.; Harbach, P. H. P.; Hauser, A. W.; Hohenstein, E. G.; Holden, Z. C.;

Jagau, T.-C.; Ji, H.; Kaduk, B.; Khistyaev, K.; Kim, J.; Kim, J.; King, R. A.; Klunzinger, P.; Kosenkov, D.; Kowalczyk, T.; Krauter, C. M.; Lao, K. U.; Laurent, A. D.; Lawler, K. V.; Levchenko, S. V.; Lin, C. Y.; Liu, F.; Livshits, E.; Lochan, R. C.; Luenser, A.; Manohar, P.; Manzer, S. F.; Mao, S.-P.; Mardirossian, N.; Marenich, A. V.; Maurer, S. A.; Mayhall, N. J.; Neuscamman, E.; Oana, C. M.; Olivares-Amaya, R.; O'Neill, D. P.; Parkhill, J. A.; Perrine, T. M.; Peverati, R.; Prociuk, A.; Rehn, D. R.; Rosta, E.; Russ, N. J.; Sharada, S. M.; Sharma, S.; Small, D. W.; Sodt, A.; Stein, T.; Stück, D.; Su, Y.-C.; Thom, A. J. W.; Tsuchimochi, T.; Vanovschi, V.; Vogt, L.; Vydrov, O.; Wang, T.; Watson, M. A.; Wenzel, J.; White, A.; Williams, C. F.; Yang, J.; Yeganeh, S.; Yost, S. R.; You, Z.-Q.; Zhang, I. Y.; Zhang, X.; Zhao, Y.; Brooks, B. R.; Chan, G. K. L.; Chipman, D. M.; Cramer, C. J.; Goddard, W. A.; Gordon, M. S.; Hehre, W. J.; Klamt, A.; Schaefer, H. F.; Schmidt, M. W.; Sherrill, C. D.; Truhlar, D. G.; Warshel, A.; Xu, X.; Aspuru-Guzik, A.; Baer, R.; Bell, A. T.; Besley, N. A.; Chai, J.-D.; Dreuw, A.; Dunietz, B. D.; Furlani, T. R.; Gwaltney, S. R.; Hsu, C.-P.; Jung, Y.; Kong, J.; Lambrecht, D. S.; Liang, W.; Ochsenfeld, C.; Rassolov, V. A.; Slipchenko, L. V.; Subotnik, J. E.; Van Voorhis, T.; Herbert, J. M.; Krylov, A. I.; Gill, P. M. W.; Head-Gordon, M., Advances in molecular quantum chemistry contained in the q-chem 4 program package. *Mol. Phys.* **2015,** *113*, 184-215.

7. Hanwell, M. D.; Curtis, D. E.; Lonie, D. C.; Vandermeersch, T.; Zurek, E.; Hutchison, G. R., Avogadro: An advanced semantic chemical editor, visualization, and analysis platform. *J. Cheminform.* **2012,** *4*, 17.

8. Marcus, R. A., On the theory of oxidation-reduction reactions involving electron transfer. I. *J. Chem. Phys.* **1956,** *24*, 966-978.

9. Hartnett, P. E.; Mauck, C. M.; Harris, M. A.; Young, R. M.; Wu, Y.-L.; Marks, T. J.; Wasielewski, M. R., Influence of anion delocalization on electron transfer in a covalent porphyrin donor-perylenediimide dimer acceptor system. *J. Am. Chem. Soc.* **2017,** *139,* 749-756.

10. Phelan, B. T.; Zhang, J.; Huang, G.-J.; Wu, Y.-L.; Zarea, M.; Young, R. M.; Wasielewski, M. R., Quantum coherence enhances electron transfer rates to two equivalent electron acceptors. *J. Am. Chem. Soc.* **2019,** *141*, 12236-12239.